Ocean acidification enhances primary productivity and nocturnal carbonate dissolution in intertidal rock pools

Narimane Dorey[1, †], Sophie Martin[2], Lester Kwiatkowski[3]

[1] LMD-IPSL, CNRS, École Normale Supérieure/PSL Res. Univ, École Polytechnique, Sorbonne Université, Paris, 75005, France

[2] CNRS, Sorbonne Université, Laboratoire Adaptation et Diversité en Milieu Marin, UMR 7144, Station Biologique de Roscoff, Place Georges Teissier, 29680 Roscoff, France

[3] LOCEAN Laboratory, Sorbonne Université-CNRS-IRD-MNHN, Paris, 75005, France

[†] Correspondence to: Narimane Dorey

École Normale Supérieure,

Département de Géosciences,

24 rue Lhomond, 75005 Paris, France

E-mail: narimane.dorey@gmail.com

ABSTRACT

Human CO_2 emissions are modifying ocean carbonate chemistry, causing ocean acidification, and likely already impacting marine ecosystems. In particular, there is concern that coastal, benthic calcifying organisms will be negatively affected by ocean acidification, a hypothesis largely supported by laboratory studies. The inter-relationships between carbonate chemistry and marine calcifying communities *in situ* are complex and natural mesocosms such as tidal pools can provide useful community-level insights. In this study, we manipulated the carbonate chemistry of intertidal pools to investigate the influence of future ocean acidification on net community production (NCP) and calcification (NCC) at emersion. Adding CO_2 at the start of the tidal emersion to simulate future acidification (+1500 µatm pCO_2, target pH: 7.5) modified net production and calcification rates in the pools. By day, pools were fertilized by the increased CO_2 (+20 % increase in NCP, from 10 to 12 mmol O_2 m^{-2} hr^{-1}), while there was no measurable impact on NCC. During the night, pools experienced net community dissolution (NCC < 0), even in present-day conditions, when waters were supersaturated with regards to aragonite. Adding CO_2 in the pools increased nocturnal dissolution rates by 40% (from -0.7 to -1.0 mmol $CaCO_3$ m^{-2} hr^{-1}) with no consistent impact on night community respiration. Our results suggest that ocean acidification is likely to alter temperate intertidal community metabolism on sub-daily timescales, enhancing both diurnal community production and nocturnal calcium carbonate dissolution.

SHORT SUMMARY

Human CO_2 emissions are modifying ocean carbonate chemistry, causing ocean acidification, and likely already impacting marine ecosystems. Here, we added CO_2 in intertidal pools at the start of emersion to investigate the influence of future ocean acidification on net community production (NCP) and calcification (NCC). By day, adding CO_2 fertilized the pools (+20 % NCP). By night, pools experienced net community dissolution, a dissolution that was further increased (+40 %) by the CO_2 addition.

Keywords: Ocean acidification, calcification, coralline algae, mesocosms, primary production, temperate community, tidal pool

INTRODUCTION

The ongoing increase of anthropogenic carbon dioxide (CO_2) in the atmosphere and the ocean – resulting in ocean acidification - is likely to create adverse living conditions for marine coastal communities (IPCC, 2019). Ocean acidification is projected to further decrease average surface pH by up to 0.4 units by 2100 (scenario RCP8.5, Kwiatkowski et al., 2020), and is identified as a major threat to marine ecosystems (IPCC, 2019). Lower seawater pH has significant effects on marine organisms physiology and fitness: from altered survival and reduced growth (see review by Kroeker et al. 2013), to changes in pH homeostasis (e.g., Kottmeier et al., 2022), metabolic rates, and energy trade-offs (e.g., Dorey et al., 2013; Pan et al., 2015) and reduced feeding efficiency (e.g., Stumpp et al., 2013). Marine calcifiers - the builders of calcified structures ($CaCO_3$) - have been a focus of ocean acidification research due to the sensitivity of calcification to the carbonate saturation state (Ω), defined as follows:

$$\Omega = [Ca^{2+}]\,[CO_3^{2-}]/K'_{sp}$$

where K'_{sp} is the stoichiometric solubility product for the considered carbonate polymorph (i.e., Ω_a for aragonite or Ω_c for calcite). The saturation state depends on temperature, pH, and pressure (lower Ω when pH or temperature decreases and pressure increases). When $\Omega < 1$, inert carbonate minerals tend to dissolve. The polymorphs composing the calcified structure like calcite and to a greater extent aragonite and high-magnesium calcite, are prone to dissolution when pH decreases. For instance, in Atlantic surface waters (at 20°C), saturation state equilibrium ($\Omega = 1$) is reached at pH 7.3 (pCO_2 = 2650 µatm) for calcite but at pH 7.6 (1250 µatm) for aragonite. For high-magnesium calcite, experiments from (Yamamoto et al., 2012) demonstrate that inert (dead) high-magnesium calcite from coralline algae passively dissolves at Ω_a values between 3.0 and 3.2 (also see Ries et al. 2016). Organisms with calcified structures are thus likely to experience reduced net calcification due to ocean acidification, both through enhanced dissolution, and reduced gross calcification rates.

Aside from acidifying the ocean (increased H^+), increased ocean CO_2 uptake could affect the productivity of algae and marine plants. As CO_2 dissolves in the ocean, the dissolved inorganic carbon (DIC: CO_2, HCO_3^- and CO_3^{2-}) concentration increases. DIC is the substrate for marine photosynthesis (mainly CO_2 and HCO_3^-), and as such, it can limit photosynthetic rates when scarce.

In algae and marine plants that are carbon limited (permanently or periodically), elevated DIC could also directly increase photosynthetic rates and Mackey et al., (2015) propose that these rates could be further increased by the higher concentration gradient between water and the photosynthetic cells. However, the authors point out that while positive effects are theoretically expected, they may be small, specific to species' biology and the environment they live in, and difficult to predict (see also Hurd et al., 2019). In terrestrial ecosystems, the Intergovernmental Panel on Climate Change defines CO_2 fertilization as 'the enhancement of plant growth as a result of increased atmospheric CO_2 concentration' (Jia et al., 2019) and reports that CO_2 fertilization has likely already happened, although the magnitude of this effect depends on the plants, or assemblages/ecosystems considered (and on other factors constraining growth).

The response of single species to changes such as ocean acidification and increased DIC concentrations are often insufficient to predict community-level impacts. Ecological interactions such as competition or predation can affect the outcome of perturbation experiments (Kroeker et al., 2012). For instance, Paiva et al. (2021) showed that the laboratory growth of an isopod species was an order of magnitude slower than when raised in the presence of other species from its community. In another study, Legrand et al. (2019) showed that the presence of grazers increased coralline algal calcification (+50% in winter and +100% in summer), but when grazers were combined with ocean acidification, algal calcification decreased more than with acidification alone. Not taking into account such interactions can therefore result in poorly characterizing the effects of ocean acidification. Furthermore, while critical for a mechanistic understanding of the processes affecting marine biota, laboratory studies are seldom realistic. Typically performed in controlled, simplified, and stable conditions (e.g., with respect to temperature and food), laboratory studies can better assess the effect of pH alone (Widdicombe et al., 2010). However exposure to a stable pH (e.g., 7.6 vs. 8.0), fails to reflect the daily and seasonal variability observed in natural ecosystems, in particular coastal ones (Torres et al., 2021). Natural mesocosm perturbation experiments are thus essential tools to investigate future changes in variable and complex ecosystems, difficult to capture in the lab (Barry et al., 2010; Andersson et al., 2015).

Most *in situ* mesocosm experiments investigating the effect of ocean acidification have been conducted on planktonic communities, kept in large "bags" equilibrated to the desired pH (Riebesell et al., 2013). These studies demonstrate that adding CO_2 can significantly change the

organization of the plankton community (Spisla et al., 2021), and increase autotrophic biomass in high-nutrient conditions (Schulz et al., 2013). Due to the technical challenges, however, benthic calcifying communities are seldom manipulated this way *in situ* (Widdicombe et al., 2010). Two such manipulation experiments are the studies by Albright et al. (2016, 2018), where the authors used NaOH and CO_2 to reproduce pre-industrial and future pH conditions on a coral reef and found evidence that reef growth had been reduced by 7% over the industrial era and was likely to decline further. Other studies have investigated such community-level effects by either simulating "artificial", simpler, assemblages in laboratory setups (e.g., Cox et al., 2015; Pansch et al., 2016) or using phenomena such as natural CO_2 vents. For instance, in the vents of Ischia, as pH decreases, the presence of calcifying species declines (see review by Foo et al., 2018). Alternatively, Kwiatkowski et al. (2016) used locally-induced acidification due to respiration (no CO_2 addition) in tidal pools, a naturally closed system, and demonstrated that nighttime dissolution of these communities was positively correlated with Ω. Here, we used tidal pools of the English Chanel as ephemeral mesocosms, where we modified carbonate chemistry conditions at the start of emersion through CO_2 addition.

Temperate rocky tidal pools - or rockpools - are highly dynamic systems that have been long studied by naturalists since they are easy to reach and their ecosystem structure generally resemble subtidal benthic communities (Ganning, 1971). Tidal pool organisms from the upper shore, well-adapted to pool conditions, form typical benthic communities: often low in diversity, they consist of a few characteristic macroalgal (e.g., *Ulva sp.*) and animal species (e.g., limpets). In winter, red macroalgae – including calcifying algae – often dominate the pools and while they do not disappear in summer, a bloom of soft green macroalgae is generally observed during the warm season. Temperature, salinity, oxygen, and pH in the pools are extremely variable, often far outside the seasonal range of nearby free-flowing seawater (Legrand et al., 2018a; Morris and Taylor, 1983). Tidal pools generally emerge from the ocean twice a day in regions of semidiurnal tides with the duration dependent on shore location and the tidal coefficient. On short timescales tidal pools act as closed systems, with carbonate chemistry easily manipulated and temporal changes reflecting *in situ* community metabolism (no water mass transport and negligible air-sea gas exchange).

In the present study, we used tidal pools as natural mesocosms to investigate the effect of ocean acidification on communities dominated by calcifying red algae. We measured diurnal and

nocturnal net community calcification and production (or respiration) following CO_2 addition across three seasons (winter, spring, and summer), to assess how tidal pool community metabolism may respond to end of the 21st century high ocean acidification (pH 7.5).

MATERIAL AND METHODS

Field site

The experiments were performed on a rocky intertidal shore characterized by granitic substrate on the North coast of Brittany, France, between 2019 and 2021. The beach of Bloscon (48°43'30.0"N 3°58'10.5"W) is situated in Roscoff at the entrance of the Bay of Morlaix and has a hydrology principally affected by the waters of the English Channel and to a lesser extent the Penzé and Morlaix rivers (**Fig. 1**). This area is characterized by strong, oscillating, semidiurnal tides of up to 9 m. Temperatures are generally low in the deeper flowing water (from 9-10 °C in winter to 16-17 °C in summer), and salinity is close to that of the adjacent Atlantic (~35; see **Supp. Mat. Fig. S1** for detailed temperature and salinity data from the two nearby SOMLIT monitoring stations Estacade and Astan, a network described in Cocquempot et al., 2019).

Tidal pool characterization

For this study, we chose five tidal pools with high coverage in calcifying algae (≥ 30% of the pool surface area). Both crustose (CCA) and articulated (branching) coralline algae (ACA) were present. The field site has an eastern exposure, resulting in full morning sun and relatively early shade in the evening. Foreshore locations of the pools resulted in daily emersion year-round including during neap tides (mid-tide, approx. 5-6 m above chart datum). Pools emerged for 6-7 h during low-tide periods. During that time, pools were completely separated from the adjacent open water and their depths were effectively constant in winter (low-evaporation season), an indication that there was no seawater leakage.

The volume of each of the five pools (from 16 to 39 L; **Fig. 2**) was estimated in April 2021 at the end of the emersion period just before high-tide flooding, by measuring salinity changes when a known volume of freshwater was added and well mixed. To estimate the pools' initial volumes, we also took into consideration the measured salinity changes throughout the emersion

period to estimate evaporative losses and combined this with the volume directly lost through water sampling (see below). The pool projected area and the relative area covered by each type of algae were estimated from aerial photographs, with a scale and analyzed using ImageJ (U. S. National Institutes of Health, Bethesda, Maryland, USA, *https://imagej.nih.gov/ij*). Pool area ranged from 0.3 to 0.7 m^2 (**Fig. 2**). The pools had slightly different community composition with dominant calcifying red algae represented by *Lithophyllum incrustans* (CCA: 30 to 77 % of the benthic cover) and *Ellisolandia elongata* (ACA: 0 to 6 % of the benthic cover). The remaining pool area was either free of algal cover with only bare granitic rock visible or covered by soft macroalgae. In summer (September 2020 and 2021), the pools also hosted the green algae *Ulva sp.* and *Enteromorpha sp.* (2 to 44 % of the benthic cover: see **Supp. Mat. Pools: Fig. SP1-2,** for results detailed by season) and, in Pool E, small single branches of the brown algae *Sargassum muticum*, covering less than 0.5 % of the pool. One limit of this method of aerial photography is that it only takes into account what is visible from above (2D). These estimates may thus be biased against algae that were hidden under the green algae canopy in summer or that were in crevices/under rocks. We also noted the presence of diverse heterotrophs such as anemones, sea sponges, small gobies, and shrimps. Calcifying invertebrates were represented by four gastropod species: *Phorcus lineatus*, *Patella ulyssiponensis*, *Patella vulgata* and *Gibbula pennanti*.

Study design and seawater manipulation

Fieldwork was conducted during the low-tide emersion periods, day and night. We refer to the period from the beginning to the end of the pool emersion as a “low-tide emersion period” and to each seasonal sampling period as a “field session” (**Table 1**). We sampled during three seasons: winter (February 2020 and 2021), spring (April 2021), and summer (September 2020 and 2021). During each field session, all the pools experienced both "future" (approximately year 2100 under high emissions) and present-day (“present”, non-manipulated control) initial carbonate chemistry conditions. During each low-tide emersion period (n = 23), we randomly selected two or three pools in which we decreased pH to 7.5 at the start of the emersion. The following low-tide emersion period, this was reversed and pools that had been subject to present-day conditions in the previous low-tide emersion period were subject to future conditions and *vice versa*. However, due to diverse constraints, in two of the 23 emersion periods all the pools were left under present-day conditions.

Table 1: Sampling schedule: The dates of each field session are presented. Pools were monitored throughout multiple low-tide emersion periods (diurnal and nocturnal).

		Low-tide emersion periods (N)	
Season	**Dates**	**Diurnal**	**Nocturnal**
Winter	14-17 February 2020	2	0
	9-19 February 2021	8	2
Spring	28-29 April 2021	2	0
Summer	2-11 September 2020	5	1
	6-9 September 2021	0	3

In this experiment, we compared "present" and "future" seawater carbonate chemistry conditions. To simulate "future" carbonate chemistry conditions, we added small volumes of CO_2-enriched seawater (total of ~100-200 mL) at the start of the emersion period in 50 mL increments until the well-mixed pool water reached the desired pH levels (pH = 7.5, reached in less than 10 min.). CO_2-enriched seawater was prepared by super-saturating adjacent seawater in CO_2 using a high-pressure CO_2 cylinder.

Sampling and measurement of seawater parameters

***Temperature, salinity, pH, oxygen, and ammonium*:** From the start of the emersion period, we measured five parameters periodically using HACH-Lange (Loveland, USA) probes: temperature, pH_T (IntelliCAL PHC101, accuracy: ± 0.02 pH units), salinity (conductivity probe IntelliCAL CDC401, ± 0.1 units), oxygen concentration (optical sensor IntelliCAL LDO101, accuracy: ± 0.1 mg L^{-1} for 0 to 8 mg L^{-1}, ± 0.2 mg L^{-1} for greater than 8 mg L^{-1}, maximum 22 mg L^{-1}) and NH_4^+ concentration (ion selective electrode IntelliCAL ISENH4181, range: 0.018 - 9000 mg L^{-1} NH_4^+-N). Pools were well-mixed before any measurement to assure no influence of gradients forming in the pools. The measurement frequency during the emersion periods was every 15-20 min during the day (n = 1392) and reduced to once an hour at night (n = 159), when temperature, pH and light variations were limited or absent. pH was calibrated on the total scale (pH_T) using TRIS (2-amino-2-hydroxy-1,3-propanediol) and AMP (2-aminopyridine) buffer solution with a salinity of 35.0, following the recommendations from (Dickson et al., 2007).

Total alkalinity: Discrete samples for total alkalinity (TA) analysis were collected hourly. The average time between two samples was 1.0 ± 0.2 hours (n = 492, median = 1.0) during daytime and 1.4 ± 0.9 hours (n = 135, median = 1.0) during nighttime. Seawater (150 mL) was filtered with 0.7 µm GF/F borosilicates filters directly after sampling. These samples were stored in a dark cool box until the end of the tide (max. 7 h). Upon return to the lab, they were stored at 4°C in the dark until they were either analyzed within the week or poisoned with 50 µL of saturated $HgCl_2$ (see "*sample processing*"). TA was assessed potentiometrically using 50.0 ± 0.5 g of seawater and a semi-automated titration system (0.1 M HCl, Titrino 848 plus by Metrohm, Switzerland; electrode calibrated on the National Bureau of Standards scale). TA was determined using Gran titration (Gran, 1952) according to the method of Haraldsson et al. (1997) and verified against reference standards provided by A. Dickson (Scripps Institute of Oceanography, University of South California, San Diego, United States). TA samples were analyzed with single (n= 312) or duplicate (n = 320) measurements (the median of the standard deviation between duplicates was 1.05 µmol kg^{-1}). TA was salinity-normalized before further calculations, to take into account possible dilution from rain or concentration from evaporation.

To take into account the influence of the changes in nutrients (NO_3^-, NO_2^-, PO_4^{3-} and NH_4^+) on the changes in TA (Gazeau et al., 2015), we sampled seawater for nutrients in winter (February 2020) and summer (September 2020). Samples were taken during the day at the start and end of the emersion periods in the five pools. Around 60 mL of seawater was immediately filtered on 0.2 µm cellulose filters, stored in 125 mL polyethylene bottles in a cool dark box (max. 7h), and then frozen at -20 °C until analysis. Nutrient concentrations were obtained using an AA3 auto-analyzer (Seal Analytical) using the method from Aminot & Kérouel (2007). Changes in nutrient concentrations were near-negligible contributions to TA changes throughout a low-tide emersion period (< 6 µmol kg^{-1} i.e., < 2% of the observed change in TA, see full details in **Supp. Mat. Nutrients**) and thus are ignored here.

Light measurements: Surface irradiance (photosynthetically active radiation, PAR) was continuously recorded (every minute) during experiments at the field station, using a Li-Cor flat quantum light sensor (LI-190R) and logger (LI-1500, LI-COR, Germany).

Adjacent waters: Temperature, salinity, pH and TA (n = 5) were similarly sampled and measured at the sampling site during ebb tide, for the three seasons.

Carbonate chemistry calculations

The carbonate system parameters (e.g., pCO_2, DIC concentration, CO_3^{2-} concentration, and Ω_a, the aragonite saturation state) were calculated from the measurements of pH_T, TA, temperature and salinity using the *R* package *seacarb* (Gattuso et al., 2021) with the default dissociation constants recommended by Dickson et al. (2007), except for the low temperatures encountered in February 2021 where the refined constants of Sulpis et al. (2020) were used. When salinity decreased by more than 1.5 units per hour, data were excluded to avoid rain effects in the present study. When calculated DIC and Ω_a were negative, likely due to inaccuracies in the measurement and computation of the carbonate system, values were approximated to be 0 (7/627 values). The air-sea gas fluxes due to net diffusive transport were considered to be negligible in the pools (see detailed explanation the *interactive discussion*).

Biological activity calculations

The rates of Net Community Calcification (NCC; mmol $CaCO_3$ m^{-2} h^{-1}) and Net Community Production (NCP) or Community Respiration (CR; mmol O_2 m^{-2} h^{-1} or mmol C m^{-2} h^{-1}) were calculated between two consecutive sampling times. These rates respectively represent the measured changes of net $CaCO_3$ precipitation and net organic carbon production (or oxygen consumption) by the community. Positive NCC represents net $CaCO_3$ precipitation (gross precipitation > dissolution) and negative rates represent net dissolution (dissolution > precipitation). NCP is positive when the community primary production exceeds respiration and negative when community primary production is less than respiration. We use CR for nights, when there is no primary production (oxygen consumption and carbon release only).

NCC was calculated using the alkalinity anomaly method (Smith and Key, 1975). Briefly, for each mol of $CaCO_3$ precipitated, two moles of HCO_3^- combine with Ca^{2+}, and TA decreases by two moles (*Eq. 1*). Two independent estimates of NCP (or CR) were calculated, one derived from changes in ΔO_2 (NCP_{O2} or CR_{O2}) and one derived from ΔDIC and NCC (NCP_{DIC} or CR_{DIC}).

NCC and NCP (or CR) were thus calculated as follows:

$$\mathrm{NCC} = \frac{\Delta TA}{2\Delta t} \times \frac{V}{S} \qquad (1)$$

$$NCP\ (or\ CR)_{O2} = \frac{\Delta O_2}{\Delta t} \times \frac{V}{S} \quad (2)$$

$$NCP\ (or\ CR)_{DIC} = \frac{-\Delta DIC}{\Delta t} \times \frac{V}{S} - NCC \quad (3)$$

with ΔTA (mmol L^{-1}), ΔDIC (mmol L^{-1}) and ΔO_2 (mmol L^{-1}) the change in concentration of TA, DIC and O_2, between consecutive samples and Δt the duration between consecutive samples (h), V pool volume (L), S the pool surface area (m^2).

Up to seven NCC and NCP (or CR) rates were calculated for each pool during each emersion period (one per hour). These rates were used to investigate the direct correlation between biological activity and environmental factors such as light intensity or Ω_a.

Rates calculated this way are however not independent from each other (i.e., the rate measured at t+2 is dependent on the rate at t+1), limiting further statistical analyses on the effect of the treatment. This is why, to investigate the effect of pH treatment ("present" vs. "future") on community biological activity, we also calculated NCC and NCP or CR using linear regressions (NCC_{lm} and NCP_{lm} or CR_{lm}) between TA, [DIC] and [O_2] and time after the start of the emersion period (for detailed results of the regressions, e.g., goodness-of-fit, see **Supp. Mat. LM1-3**). The few data from diurnal tides that were taken after sunset were excluded from these regressions. For oxygen, data were limited to the first three hours of emersion as high O_2 concentrations (>22 mg L^{-1}) and supersaturation (>200 %) led to inaccurate measurements and/or possible oxygen degassing afterwards (see **Supp. Mat. LM2**). This regression approach provides a single estimate of the rate of NCC, NCP_{DIC} (or CR_{DIC}) and NCP_{O2} (or CR_{O2}) for each pool during each emersion period (n = 17 diurnal and 6 nocturnal low-tide emersion periods x 5 pools = 115). These rates were then used in generalized linear mixed models (GLMM) to assess the effect of pH treatment on diurnal and nocturnal biological activity (see "*statistical analyses*" below).

We calculated community calcification and production budgets (respectively CCB and CPB) at emersion as an indication of the night/day balance in calcification and production: when CCB/CPB is positive the pool community calcifies/produces more by day than they dissolve/respire at night. Both were calculated for winter (February 2020 and 2021) and summer (September 2020 and 2021) for each pool as follows:

$$\mathrm{CCB} = NCC_D + NCC_N \quad (4)$$

$$\mathrm{CPB} = NCP_D + CR_N \quad (5)$$

with NCC_D and NCP_D (> 0) the average diurnal NCC and NCP for a given pool for a treatment and a season and NCC_N and CR_N (< 0) the average nocturnal NCC and dark respiration for the same conditions. Three approaches were used for estimating CPB, given the uncertainties of each NCP estimate (see discussion): (1) O_2-derived estimates of NCP (CPB_{O2}), (2) DIC- derived estimates (CPB_{DIC}) and (3) a "mixed" approach that combined nocturnal CR_{O2} and diurnal NCP_{DIC} (CPB_m), under the assumption that one mol of carbon is produced/consumed when one mol of O_2 is produced/consumed. Although CPB resemble gross community production in the way the rates are calculated (difference between light and dark net production/respiration rates), if one wanted to reuse these rates for gross community production, they should be do so with care due to differences in night and day temperature (see extended discussion on this subject in Bracken et al., 2022). The treatment effect was assessed on CCB and CPB by comparing the change due to the "future" treatment in each pool.

Statistical analyses

All data are presented as mean ± standard deviation (SD). The analyses were made using the software R (R Core Team, 2017). The level of significance used was 5%. Because data were measured on the same five pools but on different days for different treatments, we used GLMM to test for the effect of treatment on NCC_{lm} and on O_2 and DIC-derived NCP_{lm} (or CR_{lm}), assigning sampling days (i.e., low-tide emersion periods) as the random factor and pools (five levels), mean temperature of the pool during low-tide emersion period (a continuous proxy for season) and treatment (*Treat*: "future" vs. "present") as fixed factors. This was performed using the *R* package *nlme* (Pinheiro et al., 2018). Models with and without standardized residuals were compared using ANOVAs and, when different, Akaike Information Criteria (AIC) was used to choose the best fitted-model of the two. For GLMM, mean daily PAR was not used as it has strong collinearity with mean daily temperature/season. We used ANOVAs to test the effect of temperature, pool and treatment on initial (averaged over the first hour of emersion) and final (averaged for > 5 hours after emersion) carbonate chemistry conditions. The normality of the data was tested using Shapiro–Wilk tests and qq-plots, while variance homogeneity was tested with Bartlett tests.

RESULTS

1/ Environmental conditions

Adjacent waters: Temperatures (and salinity) measured in the seawater adjacent to the pools were 6-7°C in winter (February; salinity S=35.0), 11-12°C in spring (April; S=35.5) and 17-18°C in summer (September; S=36.0). This seawater was characterized by average pH_T of 8.01 ± 0.06 units, total alkalinity of 2319 ± 6 µmol kg^{-1}, pCO_2 of 445 ± 69 µatm, Ω_a = 2.2 ± 0.3 and $[O_2]$ = 100 ± 1 % of air saturation (or 10.1 ± 1.5 mg L^{-1}; n=5).

Light duration and intensity: In Roscoff, day:night (i.e., no light) periods are typically 10h:14h in February, 14h:10h in April and September. Photosynthetically active radiation (PAR) was two to three times higher in spring/summer (**Fig. 3A**: April/September ~1500 µmol m^{-2} s^{-1}) than in winter (February ~500 µmol m^{-2} s^{-1}).

Carbonate chemistry conditions at the start of the emersion period (< 1h post emersion): Both for diurnal and nocturnal tides, the initial pH was significantly lower in pools with added CO_2 than in the present-day pools (Day: pH_T = 8.2 ± 0.1 vs. 7.5 ± 0.2 units; Night: 8.0 ± 0.1 vs. 7.4 ± 0.1 units for "present" and "future" pools respectively; *Treat* $p < 0.001$; detailed results in **Fig. S2-3**, **Table S1-2**). This corresponds to pCO_2 of 260 ± 100 vs. 1900 ± 835 µatm (day) and 510 ± 90 vs. 2310 ± 410 µatm (night) for pools in "present" and "future" conditions respectively. Adding CO_2 in the pools increased the mean DIC concentration by 320 µmol kg^{-1} during the day and 240 µmol kg^{-1} during the night. In "present-day" conditions, the pools started at supersaturated levels with regards to aragonite (day: Ω_a = 3.3 ± 1.3, night: 2.2 ± 0.3). Adding CO_2 significantly decreased Ω_a (Treat: $p < 0.001$, **Table S1**) leading to initial "future" conditions often undersaturated with regards to aragonite (Ω_a = 0.8 ± 0.5) by day and always undersaturated conditions by night (Ω_a = 0.6 ± 0.1). Furthermore, in "future" diurnal conditions, pools were always undersaturated with respect to aragonite from the start of the emersion period in February (Ω_a = 0.5 ± 0.2) but not in April (Ω_a = 1.1 ± 0.7) and September (Ω_a = 1.2 ± 0.5; **Table S1**). At the start of emersion, total alkalinity was 2303 ± 34 µmol kg^{-1} (similar to adjacent seawater), and uncorrelated with treatment ($p > 0.05$) and temperature ($p > 0.6$).

As data was averaged on the first hour post-emersion, the mean initial oxygen concentration calculated was already affected by NCP by day (14.0 ± 2 mg O_2 L^{-1}) and CR by night (9.5 ± 1.5 mg O_2 L^{-1}; vs. 10.1 ± 1.5 mg O_2 L^{-1} for adjacent seawater). This was also visible in CO_2 partial pressure, with lower pCO_2 than expected during the first hour post-emersion by day (262 ± 102 µatm vs. 445 ± 69 µatm for adjacent seawater) and higher pCO_2 at night (508 ± 88 µatm) in the "present-day" conditions.

2/ Diurnal tides

Diurnal pool chemistry: Starting from the aforementioned values at emersion, the pools followed a clear temporal evolution due to solar irradiance and community metabolism (**Fig. 3**). Firstly, we observed increases in salinity (+1.5 units on average, **Fig. 3A**) and temperature (+4°C in September, +6°C in April on average) in summer and spring. In winter, temperatures tended to decrease (-1.7°C on average) with air temperatures colder than that of the seawater; salinity was stable (35.5 ± 0.8).

Secondly, we observed positive NCP corroborated by a doubling in oxygen concentration (**Fig. 3A**) a few hours after the start of emersion. In parallel, the seawater DIC concentration decreased by half from the initial concentration (from 2130 ± 195 to 1140 ± 560 µmol kg^{-1}; **Fig. 3B**), the range of which largely depended on the season (**Fig. S2**). For instance, in February, DIC consumption in pool seawater averaged ~700 µmol kg^{-1} over a low-tide period, while it averaged ~1500 µmol kg^{-1} in September. Particularly extreme conditions, with DIC concentrations effectively reaching 0 µmol kg^{-1}, were observed in two of the pools, at three tides in September 2020 (see further details below in "*5/ The particular case of September 2020 tides*"). At the end of diurnal emersions, average pCO_2 was always below 100 µatm, reaching as low as 1 ± 2 µatm in September (**Fig. 3B**, **Table S1**). As a result, diurnal pH_T increased to 9.1 ± 0.6 by the end of emersion, with maximum values up to 10.3 in summer (**Fig. 3B**). At the end of a diurnal emersion period, the pools' pH was stable, reaching either a plateau or decreasing after sunset (see PAR in **Fig. 3A**). Similarly, at the end of diurnal emersion periods, Ω_a was high (5.6 ± 3.0 on average; max 10.4). Lastly, we observed a diurnal decrease in TA by 415 µmol kg^{-1} on average, indicative of net calcification.

It is noteworthy that the carbonate chemistry conditions experienced at the end of diurnal emersion converged whatever the initial treatment (**Fig. S2**, **Table S1**). For instance, while Ω_a was significantly different between treatments at the start of the emersion period, both treatments reached similar Ω_a at the end of emersion (> 5 h) of around 5.3 ± 2.2 (ANOVA: Treat: $p = 0.1$, Temp: $p = 0.002$, Pool: $p = 0.01$). There was less convergence for pH_T where, even five hours after emersion, there were still statistically significant, albeit small, differences between treatments ($p < 0.001$ for pH_T with 9.2 ± 0.6 for "present" and 9.0 ± 0.6 for "future" pools).

Diurnal biological activity: Net community production was positive during daytime, except at sunset (**Fig. 3C**). NCP was significantly correlated to light intensity (PAR) and further results for hourly NCP and their correlation to hourly averaged PAR, Ω_a and temperature can be found in the **Supp. Mat.** (**Fig. S6** and **S7**).

As expected, seasons/temperature affected net oxygen production (O_2-derived NCP_{lm}), increasing from 7 ± 3 mmol O_2 m^{-2} hr^{-1} in February to 18 ± 11 mmol O_2 m^{-2} hr^{-1} in September (**Fig. 4A** and **Table 2A**: GLMM, $p < 0.001$). CO_2 addition increased O_2-derived NCP_{lm} by 20% on average over all seasons, from 10 ± 7 mmol O_2 m^{-2} hr^{-1} in "present" conditions to 12 ± 9 mmol O_2 m^{-2} hr^{-1} ($p = 0.0015$). Net oxygen production differed across pools ($p < 0.003$), with significantly more productivity in pool C (17.6 ± 12.7 mmol O_2 m^{-2} hr^{-1}) and D (10.6 ± 5.6 mmol O_2 m^{-2} hr^{-1}), compared to the pools A, B and E (8.1 ± 4.1 mmol O_2 m^{-2} hr^{-1}).

Results are similar for DIC-derived NCP_{lm} (**Fig. 4A** and **Table 2B**), with primary production ranging from 6 ± 2 mmol C m^{-2} hr^{-1} in February up to 12 ± 5 mmol C m^{-2} hr^{-1} in September ($p < 0.001$). As for O_2-derived NCP_{lm} CO_2 addition increased DIC-derived NCP_{lm} by 20 % on average over all seasons ($p < 0.001$, **Fig. 4A**). This increase was particularly apparent in the summer, where NCP_{lm} increased from 11 ± 4 mmol m^{-2} hr^{-1} in the "present" treatment to 15 ± 5 mmol C m^{-2} hr^{-1} in the "future" treatment (+ 35 %). Productivity (NCP_{lm}) was significantly lower in pools B and E than in pool A, and significantly higher in pools C and D ($p < 0.003$).

By day, with the exception of sunset, net community calcification was positive (NCC and $NCC_{lm} > 0$: **Fig. 3C** and **4B**) and occurred in an environment that was supersaturated with regards to aragonite (**Fig. 3B**). This was with the exception of a few emersion periods in September 2020 where dissolution was observed despite high saturation state conditions (further details below).

Similar to NCP_{lm}, diurnal net calcification rates (NCC_{lm}) were strongly influenced by temperature/season (**Fig. 4B** and **Table 2C**: GLMM, $p < 0.001$) ranging from 1.2 ± 0.5 mmol $CaCO_3$ m^{-2} hr^{-1} in February to 3.3 ± 1.3 mmol $CaCO_3$ m^{-2} hr^{-1} in September. NCC hourly rates positively correlated with averaged Ω_a ($p < 0.0001$; NCC = 0.15 x Ω_a + 0.85; linear regression presented in **Fig. S7**), significantly but not strongly ($R^2 = 10\%$). CO_2 addition did not influence NCC_{lm} rates during the day ($p = 0.47$). However, NCC_{lm} did differ across pools ($p < 0.003$): rates were relatively low in pool E – lowest CCA cover (30%) – (1.4 ± 1.4 mmol $CaCO_3$ m^{-2} hr^{-1}), and high in pool D – highest CCA cover (70%) – (2.2 ± 0.8 mmol $CaCO_3$ m^{-2} hr^{-1}) compared to the three other pools (2.0 ± 1.25 mmol $CaCO_3$ m^{-2} hr^{-1}).

Table 2: Results of the generalized linear mixed-effect models for A) O_2-derived NCP_{lm} (mmol O_2 m^{-2} hr^{-1})**, B) DIC-derived NCP_{lm}** (mmol C m^{-2} hr^{-1}) **and C) NCC_{lm}** (mmol $CaCO_3$ m^{-2} hr^{-1}) **during the day and night**. The models include three fixed factors: *Temp* (mean temperature: a continuous factor), *Treat* (for CO_2 "future" treatment vs. "present", two levels) and *pools* (vs. A, five levels), and one random effect (*low-tide emersion period* or the calendar day at which the pool was measured). Significant *p*-values are highlighted in bold.

A.	**O_2-derived NCP_{lm}**		**Estimate**	**Standard Error**	***p*-value**
Day	**Intercept**		1.49	1.37	0.28
	Fixed Effects	*Temp*	0.54	0.13	**<0.001***
		Treat	1.09	0.33	**0.0015***
		Pools	A, B, E ≠ C, D		**<0.003***
	Random Effect	*Low-tide emersion period*	8.90	0.90	**<0.001***
Night	**Intercept**		2.87	0.98	**0.005***
	Fixed Effects	*Temp*	-0.43	0.06	**<0.001***
		Treat	-0.25	0.28	0.39
		Pools	A, B, D ≠ C, E		**<0.03***
	Random Effect	*Low-tide emersion period*	-3.46	0.87	**<0.001***

430

B.	DIC-derived NCP_{lm}		Estimate	Standard Error	*p*-value
Day	**Intercept**		2.3	1.08	**0.035***
	Fixed Effects	*Temp*	0.38	0.08	**<0.001***
		Treat	1.25	0.25	**<0.001***
		Pools	A ≠ B, C, D, E		**<0.003***
	Random Effect	*Low-tide emersion period*	7.7	0.7	**<0.001***
Night	**Intercept**		-0.94	1.4	0.51
	Fixed Effects	*Temp*	-0.92	0.19	0.053
		Treat	-0.25	0.28	**<0.001***
		Pools	A, B, D, E ≠ C		**0.016***
	Random Effect	*Low-tide emersion period*	1.61	0.57	**0.01***

431

C.	NCC_{lm}		Estimate	Standard Error	*p*-value
Day	**Intercept**		-0.16	0.31	0.61
	Fixed Effects	*Temp*	-0.13	0.02	**<0.001***
		Treat	0.06	0.08	0.47
		Pools	A, B, C ≠ D, E		**<0.003***
	Random Effect	*Low-tide emersion period*	-1.90	0.24	**<0.001***
Night	**Intercept**		0.64	0.26	**0.026***
	Fixed Effects	*Temp*	0.009	0.016	0.57
		Treat	0.28	0.07	**0.0017***
		Pools	A, B, C ≠ D, E		**<0.017***
	Random Effect	*Low-tide emersion period*	0.83	0.078	**<0.001***

432

3/ Nocturnal tides

Nocturnal pool chemistry: Seawater temperatures during the nights were stable (**Fig. 3A**) throughout the emersion period in summer (from 17.3 ± 0.4°C < 1 h post-emersion to 17.2 ± 0.2°C > 5 h post-emersion) and winter (from 8.4 ± 1.4°C to 7.8 ± 2.7°C in February; no April nights). We highlight the wide range of winter seawater temperatures with an exceptionally cold tidal cycle (5°C on the 13th of February 2021) due to air temperatures of 3-4°C (observations from the Île de Batz meteorological station). There was a decline in salinity at night in some winter emersion periods (**Fig. 3A**), due to high air humidity and/or rain. Data where salinity dropped by more than 1.5 units in less than an hour were removed from further analyses on net community calcification and respiration.

After five hours of emersion, O_2 concentration had decreased by half (from 10.1 ± 1.5 mg O_2 L^{-1} to 4.9 ± 3.3 mg O_2 L^{-1}) (**Fig. 3A**) due to community respiration. Simultaneously, pH_T decreased to 7.6 ± 0.2 ("present") or stayed at 7.4 ± 0.2 ("future"; **Fig. 3B and S2, Table S1**), with significant effects of pools, treatment and temperature ($p < 0.001$ for all three). DIC concentration increased by +256 µmol kg^{-1} on average over an emersion period. The range of this increase depended on the temperature and the pool: in winter (5-10°C), present-day pool seawater gained +130 µmol kg^{-1} (+60 for "future" pools) of DIC over an emersion period, when in summer they gained +370 µmol kg^{-1} for "present" ("future": +310 µmol kg^{-1}) pools (**Fig. S3**). Saturation state converged towards similar undersaturated levels at night (**Fig. 3B and S2**, **Table S1**): Ω_a stayed stable in the "future" treatment (0.7 ± 0.2 units on average) and decreased in the "present-day" treatment (-1.2 units from initial Ω_a). At the end of nocturnal emersion Ω_a were still statistically different due to the initial treatment ($p < 0.001$ for *Treat*, *Temp* and *Pools*).

Nocturnal biological activity: At night, oxygen was consumed, i.e., we observed dark respiration (CR; **Fig. 3C**). Community respiration (O_2-derived CR_{lm}) varied according to season (**Fig. 4A** and **Table 2A**: $p < 0.001$): temperature linearly increased nocturnal respiration rates from -1.0 ± 1.2 mmol O_2 m^{-2} hr^{-1} in February to -4.7 ± 1.3 mmol O_2 m^{-2} hr^{-1} in September. The CO_2 treatment did not influence night respiration ($p = 0.39$). Respiration rates were significantly influenced by pools ($p = 0.03$), probably linked to the relative biomass of heterotrophs and autotrophs; respiration was significantly higher in pool C (-4.6 ± 2.8 mmol O_2 m^{-2} hr^{-1}) and significantly lower in pool E (-2.4 ± 1.4 mmol O_2 m^{-2} hr^{-1}) than in pools A, B and D (-3.4 ± 2.1 mmol O_2 m^{-2} hr^{-1}).

Night respiration estimated using DIC and NCC was near zero (CR_{lm} = -0.2 ± 0.7 mmol m^{-2} hr^{-1}). At these low rates, uncertainties associated with much higher rates of net dissolution (negative NCC) sometimes led to spuriously positive DIC-derived CR estimates, hindering interpretation. Nevertheless, DIC-derived community respiration was ten times lower in February than in September (-0.2 ± 0.7 and -2.3 ± 1.1 mmol C m^{-2} hr^{-1} respectively), although it was not linearly driven by temperature (p = 0.053; **Fig. 4B** and **Table 2B**). Adding CO_2 to the pools influenced DIC-derived community respiration in a way that was inverse to that seen with O_2, but as stated above, this was likely an artifact of subtracting NCC from small DIC changes. As for O_2, DIC-derived CR_{lm} significantly changed depending on the pools.

At night, the pools experienced significant net community dissolution (NCC < 0: **Fig. 3C**) even when waters were supersaturated with regards to aragonite in the "present" treatment (**Fig. 3B**: Ω_a > 1). Nocturnal net dissolution rates (NCC_{lm}) were not significantly affected by temperature in the range investigated (5-18°C; **Fig. 4C** and **Table 2C**: p = 0.57). However, adding CO_2 in the pools increased net dissolution rates (p = 0.0017) from -0.7 ± 0.3 mmol $CaCO_3$ m^{-2} hr^{-1} to -1.0 ± 0.4 mmol $CaCO_3$ m^{-2} hr^{-1} (+40 %). Similarly, looking instead at hourly rates (NCC), dissolution correlated significantly (p < 0.0001) with Ω_a (NCC = 0.34 x Ω_a – 1.22; R^2 = 11 %; **Fig. S7**). The strength of this correlation depended on seasons and pools (**Fig. S8**). Net dissolution rates (NCC_{lm}) significantly differed by pool (p < 0.0017): the lowest rates were observed in pool E (-0.4 ± 0.2 mmol $CaCO_3$ m^{-2} hr^{-1}) – the pool with the lowest CCA cover –, and the highest dissolution in pool D – the pool with the highest CCA cover (-1.0 ± 0.4 vs. -0.9 ± 0.3 mmol $CaCO_3$ m^{-2} hr^{-1} for A, B and C).

4/ Influence of the treatment on CPB and CCB

Pools fixed more carbon during the day than they respired at night, i.e., the community production budget (CPB: balance between night and day) was positive in all the pools, both in winter and summer and whatever the treatment (**Fig. 5**). CPB_{DIC} and CPB_m estimates were typically lower than CPB_{O2} (in 14/20 cases and 18/20 cases respectively). The production budget was significantly lower in winter than in summer (FEB: CPB_{O2} = 3 ± 1 mmol O_2 m^{-2} h^{-1}, SEP: 7 ± 5 mmol O_2 m^{-2} h^{-1}; t-test: t = -2.4, df = 9.8, p = 0.03). Adding CO_2 increased CPB in all the pools in summer by + 3.0 ± 2.1 mmol O_2 m^{-2} h^{-1}, an increase in production by 50 to 80 % (ΔCPB; **Fig. 5**). In winter, there

was no evidence of such a "fertilization effect" across the most accurate CPB estimates for this season (CPB_{O2}, CPB_m): we only observed a significant increase in production due to CO_2 addition in two of the pools (+60 % to +120 % for A and B). For the three other pools, CPB either induced minimal changes (< 20 % for C and E) or a decrease in production (D: down to -34 %). DIC-derived ΔCPB in winter (all positive) should be interpreted with caution since some nocturnal CR_{lm} were spuriously positive in the "future" treatment (see "*nocturnal biological activity*" above).

The pools calcified more during the day than they dissolved at night (CCB > 0), both in summer and winter (**Fig. 5**). CCB was significantly lower in winter than in summer (FEB: CCB = 0.2 ± 0.2 mmol $CaCO_3$ m^{-2} h^{-1}, SEP: 1.2 ± 0.6 mmol $CaCO_3$ m^{-2} h^{-1}; t-test: t = -5.2, df = 11.7, p = 0.0002). In winter, adding CO_2 decreased CCB by more than 80 % in pools C, D, and E (**Fig. 5**). The CO_2 addition even resulted in a transition from a positive community calcification balance to dissolution in pool C (133 % change, from +0.5 to -0.2 mmol $CaCO_3$ m^{-2} h^{-1}). For the two other pools (A and B), winter CO_2 addition increased their relatively small calcification balance (A: +87 %, from 0.1 to 0.2 mmol $CaCO_3$ m^{-2} h^{-1} and B: +71 %, from 0.2 to 0.3 mmol $CaCO_3$ m^{-2} h^{-1}). In summer, changes in CCB due to treatment appeared minimal in pools A, B and E (< 15 % change) and either increased (C: +67%) or decreased (D: -57%) in the two other pools.

5/ The particular case of September 2020 tides

During diurnal tides of September 2020 (high PAR and high temperature summer conditions), we observed an unexpected phenomenon: dissolution occurred at extremely high pH_T values (9-10) in pools C and E (**Fig. 6**). Under these conditions effectively all the seawater DIC in these pools was consumed by photosynthesis and calcification (DIC ≈ 0 mmol kg^{-1}) four hours after emersion. As such, the CO_3^{2-} concentration was also effectively zero and the pools reached very low saturations states ($\Omega_a \approx 0$) despite high pH (**Fig. 6**). These conditions were quickly followed by indicators of $CaCO_3$ dissolution (increasing TA and DIC) instead of the expected diurnal precipitation. It is therefore noteworthy that dissolution may happen at high pH, and that pH and Ω can decorrelate (**Fig. 7**) in situations with high photosynthesis and limited mixing of water masses.

DISCUSSION

Temperate tidal pools are environments of extreme variability. In our pools, we observed seawater temperatures that could increase by up to 10°C in a few hours compared to the adjacent ocean. During diurnal emersion periods, oxygen concentrations doubled and pH could increase to pH 10 in present-day summer conditions. At night, pH routinely reached levels usually used as the "treatment" for ocean acidification perturbation experiments (~7.6). Organisms present in the tidal pools may therefore already be adapted or acclimatized to extreme variability in pH and saturation state, which could affect their responses to ocean acidification (Andersson et al., 2015). For example, CCA from a site with naturally high pCO_2 variability calcified ~50 % more than individuals from a nearby site of low variability when submitted to oscillating high pCO_2 treatments (Johnson et al., 2014). Here we show that, even in intertidal communities likely already acclimated or adapted to variable conditions, with potentially large phenotypic plasticity, acidification can still modify net community production and calcification rates.

Diurnal fertilization under CO_2 addition

Adding CO_2 to simulate future seawater acidification in the pools led to a diurnal fertilization effect. The community's net primary production increased by 20% on average across all seasons, which was particularly visible in summer (+ 35%), when temperatures/metabolic rates were high. Adding CO_2, we also added substrate for photosynthesis in the form of DIC (**Fig. 3B**) that the algae of the pools can assimilate, potentially supporting higher DIC use and algal primary production. This effect was apparent from the start of the emersion, suggesting a direct effect of increasing DIC concentration in the pools. It seems that photosynthesis in the pools was carbon-limited and that carbon addition therefore enhanced primary production, in winter and to an even greater extent in summer. During photosynthesis, the uptake of inorganic carbon leads to a significant decrease in DIC - even in present-day conditions. Intertidal algae are typically adapted to this with coralline algae in particular containing CCMs (CO_2 concentrating mechanisms) that allow them to achieve primary production in low DIC concentrations (Raven, 2011). Increasing seawater DIC may however promote an increase in active and/or passive CO_2 and HCO_3^- fluxes towards photosynthetic compartments. Borowitzka (1981) found that the photosynthetic rate of an intertidal CCA was highest at pH 6.5 to 7.5 (increased from pH 8.1), a change in pH that was achieved using HCl, suggesting that increased photosynthetic activity could also be linked to

552 proton gradients/pumps and/or decreased energy expenditure needed to operate CCMs rather than
553 directly related to CO_2 gradients or higher substrate availability.

554 In winter and summer, pools in present-day and future conditions were autotrophic at
555 emersion ($NCP_D > CR_N$, **Fig. 5**). If we consider the CPB as integrated diurnal NCP and nocturnal
556 CR over 24 hours (assuming equal day:night duration), this means that the pools always fixed
557 more carbon during the day than they respired at night at emersion (NCP >> CR), regardless of
558 treatment. One methodological uncertainty we highlight regarding net production is that diurnal
559 DIC-derived NCP estimations were 50 % higher than O_2-derived NCP estimates (**Fig. 3C and Fig.**
560 **4**, $NCP_{DIC} = 1.6 \pm 0.05\ NCP_{O2}$ by day; $R^2 = 75$ %). This discrepancy was far less apparent during
561 nights, when methods agreed on respiration rates ($CR_{DIC} = 1.0 \pm 0.09\ CR_{O2}$; $R^2 = 56$ %). While
562 O_2-derived NCP appears accurate during the night, O_2 production during the day is likely to have
563 been underestimated due to degassing (e.g., visible formation of oxygen bubbles at the surface of
564 algae, >150 % air saturation by day vs. < 100 % at night). Thus, estimating diurnal net production
565 using oxygen measurements may not be appropriate in algae-dominated environments such as
566 these tidal pools. Nevertheless, despite the difference in absolute NCP estimates, both approaches
567 indicate a diurnal fertilization effect.

568

569 **Nocturnal dissolution under CO_2 addition**

570 In the present study, natural mesocosms - temperate coralline-dominated tidal pools - were used
571 to investigate the effect of ocean acidification on net calcification at the community level. As we
572 observed a fertilization effect of CO_2 addition by day, we could have expected that it would also
573 enhance diurnal calcification – as photosynthesis and calcification are tightly linked (Martin et al.,
574 2013; Martin et al., 2013; Williamson et al., 2017) -, but this was not observed. Treatment had no
575 significant effect on the daytime net calcification rates, and diurnal variability in calcification
576 appears to be predominately driven by PAR, temperature, and metabolic activity (NCP). Increasing
577 metabolic rates - in turn increasing calcification rates - may have however counterbalanced any
578 calcification suppression or increased dissolution due to acidification, making its effect invisible.
579 Noisette et al. (2013) similarly found no effect of pCO_2 treatment on light calcification for *E.*
580 *elongata*. However, the authors reported a significant decrease in light calcification in *L.*
581 *incrustans*, net calcification even switched to net dissolution in 750 and 1000 µatm pCO_2
582 treatments. While our "future" treatments started at pCO_2 levels higher than 1000 µatm, the fact

583 that CO_2 addition did not influence diurnal calcification could also be due to favorable saturation
584 state conditions in the micro-environment in which calcification occurs. The diffusive boundary
585 layer (DBL) can enhance $CaCO_3$ precipitation micro-environment conditions due to the uptake of
586 CO_2/DIC for photosynthesis. For instance, in light conditions, CCA surface pH has been shown to
587 reach as high as 8.6 (Houlihan et al., 2020) in surrounding seawater at pH 7.7 (+1.1 pH units),
588 which would be highly favorable to calcification. Although there are conflicting results indicating
589 that saturation state of the ambient seawater is a key driver of coralline algal calcification, the
590 biomineralization process in coralline algae has also been shown to present a certain degree of
591 biological control (de Carvalho et al., 2017; Nash et al., 2019). Recent work using boron isotopes
592 (δ11B) as a proxy for pH showed that coralline algae have ability to elevate pH at their site of
593 calcification (Cornwall et al., 2017). But more complex interactions may also be at work, e.g.,
594 CCA may use increases in HCO_3^- (due to CO_2 dissolution) to calcify, making them more resistant
595 to ocean acidification, as suggested by Comeau et al. (2013).
596 There was net $CaCO_3$ dissolution in the pools at night (-0.7 mmol $CaCO_3$ m^{-2} hr^{-1}), even
597 when waters were still supersaturated with regards to aragonite under present-day conditions.
598 Night dissolution may be a sign that the DBL of the calcifiers inhabiting the pools is
599 undersaturated, possibly as a result of respiration. Indeed, Houlihan et al. (2020) observed that
600 nocturnal algal respiration by CCA, increased CO_2 in the DBL, decreasing pH of the DBL by 0.1
601 units. Such a small pH decrease is unlikely to explain alone an undersaturation of the calcifying
602 environment as aragonite saturation state was still above 1.2 in most of the "present-day"
603 conditions. However, given the solubility of high-Mg calcite - the mineral composing *L. incrustans*
604 and *E. elongata* in particular (Ries, 2011) - can be twice that of aragonite (Sulpis et al., 2021;
605 Yamamoto et al., 2012), it is possible that undersaturation already occurs at night for this mineral
606 even for $\Omega_a > 1$. Another reason for night dissolution might be linked to the patellid limpet, an
607 opportunistic (Schaal and Grall, 2015) and dominant grazer in rockpools, that can be particularly
608 active at night(Lorenzen, 2007). Encrusting coralline algae can be an important food source for
609 these herbivores and the large percentage of grazed coralline algal $CaCO_3$ in their gut (Maneveldt
610 et al., 2006) could dissolve easily at night.
611 Adding CO_2 (from 445 to 1500-2000 µatm) at the start of emersion significantly increased
612 net dissolution (NCC_{lm}), by 40 % in summer and 70 % in winter. In a previous single-species
613 experiment, Noisette et al. (2013) demonstrated that - for *L. incrustans* from an area close to our

site – dark dissolution doubled with increasing pCO_2 (1000 µatm vs. 380 µatm), unlike *E. elongata*, for which there was no effect of pCO_2: the ACA even calcified in the dark up to 750 µatm (see also similar results from Egilsdottir et al., 2013). Since *L. incrustans* is the major calcifying species of the tidal pools we studied, it is likely this species drives the results we observed at the pool community scale. Regardless of the treatment, nocturnal net dissolution rates (NCC) were also significantly correlated with Ω_a, results similar to those found by Kwiatkowski et al. (2016) in temperate tidal pools of California, without CO_2 addition.

In summer, pools in present-day and future conditions were precipitative (CCB > 0), meaning that diurnal net calcification exceeded nocturnal net dissolution, regardless of treatment. Adding CO_2 in summer did not consistently change CCB, with most pools showing little change in CCB due to treatment. By contrast, in the colder winter, the calcification budget was at least 50 % lower than in summer ("present"), with some pools that had comparable net calcification during the day to net dissolution at night. During this season, adding CO_2 had variable impacts on CCB, decreasing it in three of the pools by more than 80 % and increasing relatively small CCB in two. These variable effects may be due to differences in community composition and highlight the difficulty in generalizing the results of natural mesocosm manipulations in which the initial community composition is not controlled. Nevertheless, we expected CO_2 addition to have a greater negative effect in winter (more dissolution) than in summer, with saturation states being lower due to colder temperatures, making it more of a "crucial"/ "bottleneck" season. This emphasizes the need to study the effect of ocean acidification across seasons and temperature ranges, especially given the associated changes in algal community composition and metabolic activity.

A limit of the CCB in the current study is that we only considered the tidal pools as closed (emersed) systems. However, in an acidifying ocean, tidal pool communities are submersed for nearly 12 hours per day, resulting in long exposure to low pH. More accurate and realistic budgets would need to integrate these immersion periods, which might have additive negative effects on calcification (see e.g., Legrand et al., 2018b for tidal assemblage experiments on net production/respiration).

Instances of aragonite undersaturation at high pH

An unexpected phenomenon happened in the pools C and E in summer: although we measured very high pH values, we observed that total alkalinity suddenly increased, a sign of fast net dissolution. When we then computed the carbonate chemistry, the saturation states were

surprisingly low ($\Omega_a = 0$ for $pH_T = 10$), which was due to near-zero DIC concentrations – and thus near-zero CO_3^{2-} concentrations. In these particular conditions, which occurred towards the end of the tidal emersion period, any $CaCO_3$ precipitation was less than dissolution; precipitation may even have been impossible due to a lack of DIC substrate. In intertidal pools with a high density of *Zostera marina*, Miller & Kelley (2021) observed a similar decoupling between pH and Ω_a with increases in pH not leading to an increase in saturation state at high pH values due to a lack of DIC/CO_3^{2-}. In our study, we observed even more drastic decoupling between expected changes in pH, Ω_a and NCC, with some of the fastest net dissolution rates observed at very high pH and very low Ω_a values that were a consequence of near complete consumption of DIC by community production (**Fig. 7**). Macroalgae cultivation has been proposed as a method of bioremediation to local acidification, in particular to improve aquaculture environments (e.g., Bergstrom et al., 2019; Gao & Beardall, 2022): increase in algal or marine plant cover would reverse or buffer the negative effects of acidification on heterotroph calcifiers. Our results and those of Miller & Kelley (2021) suggest that phytoremediation should not consider pH as the sole indicator for "acidification remediation", and that periodical decreases in saturation state in macroalgae- or seaweed-dominated environments in summer (and during marine heatwaves), may need to be considered for these proposed types of remediations.

Conclusion

Relative to its area, human societies are disproportionately reliant on the coastal ocean for the provision of natural resources and climate regulation. Yet our understanding of how anthropogenic carbon emissions and associated ocean acidification will influence natural coastal ecosystems and community metabolism remains limited. In the present study, we manipulated the carbonate chemistry of natural temperate intertidal pools to explore the potential impact of future ocean acidification on community-level calcification and production. We find evidence of large seasonal, diel and community-specific differences in the sensitivity of intertidal community metabolism to acidification. Diurnally, acidification was found to enhance net community production, with this "fertilization effect" indicating algal photosynthesis is naturally carbon limited in such environments at emersion. Diurnal net community calcification was unaffected by acidification. In contrast, nocturnal acidification resulted in greater net community dissolution in the intertidal pools yet had no consistent effect on community respiration. Integrated over day/night emersion

periods, the intertidal mesocosms maintained positive net community calcification and production under both present-day and future conditions. Albeit considerable differences between individual pools and strong seasonal dependencies, our results indicate that the net calcification and production of temperate intertidal communities - likely acclimated/adapted to variable conditions - could be affected by future acidification.

ACKNOWLEDGEMENTS

We thank Elsa Perruchini, Léonard Dupont, Corentin Clerc, Priscilla Le Mezo, Alban Planchat, Maud Chevalier, Anne Cornillon, Annabel Antheaume, Maïlys Roux and Clarisse Dufaux for their kind assistance with fieldwork. This project is fully funded by the CHANEL research chair: *Understanding the Linkages between the Ocean, the Carbon Cycle, and Marine Ecosystems under Climate Change*. Data presented for adjacent Atlantic waters characteristics (main text and the supplementary material) were kindly provided by the SOMLIT network database (Service d'Observation en Milieu Littoral; www.somlit.fr) on June 2022.

AUTHORS CONTRIBUTIONS

ND, SM and LK designed the experiments and ND carried them out with help from all co-authors. ND analysed the data and prepared the manuscript, with contributions from all co-authors.

COMPETING INTERESTS

The authors declare that they have no conflict of interest.

DATA AVAILABILITY

Raw data and linear regression model results are provided as supplementary in the Appendix.

BIBLIOGRAPHY:

Albright, R., Caldeira, L., Hosfelt, J., Kwiatkowski, L., Maclaren, J. K., Mason, B. M., Nebuchina, Y., Ninokawa, A., Pongratz, J., Ricke, K. L., Rivlin, T., Schneider, K., Sesboüé, M., Shamberger, K., Silverman, J., Wolfe, K., Zhu, K., and Caldeira, K.: Reversal of ocean acidification enhances net coral reef calcification, Nature, 531, 362–365, https://doi.org/10.1038/nature17155, 2016.

Albright, R., Takeshita, Y., Koweek, D. A., Ninokawa, A., Wolfe, K., Rivlin, T., Nebuchina, Y., Young, J., and Caldeira, K.: Carbon dioxide addition to coral reef waters suppresses net community calcification, Nature, 555, 516–519, https://doi.org/10.1038/nature25968, 2018.

Aminot, A. and Kérouel, R.: Dosage automatique des nutriments dans les eaux marines: méthodes en flux continu, Editions Quae, 191 pp., 2007.

Andersson, A. J., Kline, D. I., Edmunds, P. J., Archer, S. D., Bednaršek, N., Carpenter, R. C., Chadsey, M., Goldstein, P., Grottoli, A. G., Hurst, T. P., King, A. L., Kübler, J. E., Kuffner, I. B., Mackey, K. R. M., Menge, B. A., Paytan, A., Riebesell, U., Schnetzer, A., Warner, M. E., and Zimmerman, R. C.: Understanding ocean acidification impacts on organismal to ecological scales, Oceanography, 28, 16–27, 2015.

Barry, J., Hall-Spencer, J., and Tyrrell, T.: In situ perturbation experiments: natural venting sites, spatial/temporal gradients in ocean pH, manipulative in situ pCO_2 perturbations, in: Guide to best practices in ocean acidification research and data reporting, Luxembourg, 123–136, 2010.

Bergstrom, E., Silva, J., Martins, C., and Horta, P.: Seagrass can mitigate negative ocean acidification effects on calcifying algae, Sci. Rep., 9, 1932, https://doi.org/10.1038/s41598-018-35670-3, 2019.

Borowitzka, M. A.: Photosynthesis and calcification in the articulated coralline red algae *Amphiroa anceps* and *A. foliacea*, Mar. Biol., 62, 17–23, https://doi.org/10.1007/BF00396947, 1981.

Bracken, M. E. S., Miller, L. P., Mastroni, S. E., Lira, S. M., and Sorte, C. J. B.: Accounting for variation in temperature and oxygen availability when quantifying marine ecosystem metabolism, Sci. Rep., 12:825, https://doi.org/10.1038/s41598-021-04685-8, 2022.

de Carvalho, R. T., Salgado, L. T., Amado Filho, G. M., Leal, R. N., Werckmann, J., Rossi, A. L., Campos, A. P. C., Karez, C. S., and Farina, M.: Biomineralization of calcium carbonate in the cell wall of Lithothamnion crispatum (Hapalidiales, Rhodophyta): correlation between the organic matrix and the mineral phase, J. Phycol., 53, 642–651, https://doi.org/10.1111/jpy.12526, 2017.

Cocquempot, L., Delacourt, C., Paillet, J., Riou, P., Aucan, J., Castelle, B., Charria, G., Claudet, J., Conan, P., Coppola, L., Hocdé, R., Planes, S., Raimbault, P., Savoye, N., Testut, L., and Vuillemin, R.: Coastal ocean and nearshore observation: a French case study, Front. Mar. Sci., 6, 2019.

Comeau, S., Carpenter, R. C., and Edmunds, P. J.: Coral reef calcifiers buffer their response to ocean acidification using both bicarbonate and carbonate, Proc. R. Soc. B Biol. Sci., 280, 20122374, https://doi.org/10.1098/rspb.2012.2374, 2013.

Cornwall, C. E., Comeau, S., and McCulloch, M. T.: Coralline algae elevate pH at the site of calcification under ocean acidification, Glob. Change Biol., 23, 4245–4256, https://doi.org/10.1111/gcb.13673, 2017.

738 Cox, T. E., Schenone, S., Delille, J., Díaz-Castañeda, V., Alliouane, S., Gattuso, J.-P., and Gazeau, F.: Effects
739 of ocean acidification on *Posidonia oceanica* epiphytic community and shoot productivity, J. Ecol., 103,
740 1594–1609, https://doi.org/10.1111/1365-2745.12477, 2015.

741 Dickson, A., Sabine, C. L., and Christian, J. R.: Guide to best practices for ocean CO_2 measurements, PICES
742 Special Publication 3; 191 pp, 2007.

743 Dorey, N., Lançon, P., Thorndyke, M., and Dupont, S.: Assessing physiological tipping point of sea urchin
744 larvae exposed to a broad range of pH, Glob. Change Biol., 19, 3355–3367,
745 https://doi.org/10.1111/gcb.12276, 2013.

746 Egilsdottir, H., Noisette, F., Noël, L. M.-L. J., Olafsson, J., and Martin, S.: Effects of pCO_2 on physiology
747 and skeletal mineralogy in a tidal pool coralline alga *Corallina elongata*, Mar. Biol., 160, 2103–2112,
748 https://doi.org/10.1007/s00227-012-2090-7, 2013.

749 Foo, S., Byrne, M., Ricevuto, E., and Gambi, M. C.: The carbon dioxide vents of Ischia, Italy, a natural
750 system to assess impacts of ocean acidification on marine ecosystems: An overview of research and
751 comparisons with other vent systems, Oceanogr. Mar. Biol. Annu. Rev., 56, 237–310,
752 https://doi.org/10.1201/9780429454455-4, 2018.

753 Ganning, B.: Studies on chemical, physical and biological conditions in swedish rockpool ecosystems,
754 Ophelia, 9, 51–105, https://doi.org/10.1080/00785326.1971.10430090, 1971.

755 Gao, K. and Beardall, J.: Using macroalgae to address UN Sustainable Development goals through CO_2
756 remediation and improvement of the aquaculture environment, Appl. Phycol., 3, 360–367,
757 https://doi.org/10.1080/26388081.2022.2025617, 2022.

758 Gattuso, J.-P., Epitalon, J.-M., Lavigne, H., and Orr, J.: seacarb: seawater carbonate chemistry with R. R
759 package version 3.2.16 http://CRAN.R-project.org/package=seacarb, 2021.

760 Gazeau, F., Urbini, L., Cox, T., Alliouane, S., and Gattuso, J.: Comparison of the alkalinity and calcium
761 anomaly techniques to estimate rates of net calcification, Mar. Ecol. Prog. Ser., 527, 1–12,
762 https://doi.org/10.3354/meps11287, 2015.

763 Gran, G.: Determination of the equivalence point in potentiometric titrations. Part II, The Analyst, 77,
764 661, https://doi.org/10.1039/an9527700661, 1952.

765 Haraldsson, C., Anderson, L. G., Hassellöv, M., Hulth, S., and Olsson, K.: Rapid, high-precision
766 potentiometric titration of alkalinity in ocean and sediment pore waters, Deep Sea Res. Part Oceanogr.
767 Res. Pap., 44, 2031–2044, https://doi.org/10.1016/S0967-0637(97)00088-5, 1997.

768 Houlihan, E. P., Espinel-Velasco, N., Cornwall, C. E., Pilditch, C. A., and Lamare, M. D.: Diffusive boundary
769 layers and ocean acidification: Implications for sea urchin settlement and growth, Front. Mar. Sci., 7,
770 2020.

771 Hurd, C. L., Beardall, J., Comeau, S., Cornwall, C. E., Havenhand, J. N., Munday, P. L., Parker, L. M., Raven,
772 J. A., McGraw, C. M., Hurd, C. L., Beardall, J., Comeau, S., Cornwall, C. E., Havenhand, J. N., Munday, P. L.,
773 Parker, L. M., Raven, J. A., and McGraw, C. M.: Ocean acidification as a multiple driver: how interactions

between changing seawater carbonate parameters affect marine life, Mar. Freshw. Res., 71, 263–274, https://doi.org/10.1071/MF19267, 2019.

IPCC: IPCC Special Report on the Ocean and Cryosphere in a Changing Climate, edited by: Pörtner, H. O., Roberts, D., Masson-Delmotte, V., and Zhai, P., Cambridge University Press, UK, 755 pp., https://doi.org/10.1017/9781009157964, 2019.

Jia, G., E. Shevliakova, P. Artaxo, N. De Noblet-Ducoudré, R. Houghton, J. House, K. Kitajima, C. Lennard, A. Popp, A. Sirin, R. Sukumar, and L. Verchot: Land–climate interactions., in: Climate Change and Land: an IPCC special report on climate change, desertification, land degradation, sustainable land management, food security, and greenhouse gas fluxes in terrestrial ecosystems, 2019.

Johnson, M. D., Moriarty, V. W., and Carpenter, R. C.: Acclimatization of the Crustose Coralline Alga Porolithon onkodes to Variable pCO2, PLOS ONE, 9, e87678, https://doi.org/10.1371/journal.pone.0087678, 2014.

Kottmeier, D. M., Chrachri, A., Langer, G., Helliwell, K. E., Wheeler, G. L., and Brownlee, C.: Reduced H+ channel activity disrupts pH homeostasis and calcification in coccolithophores at low ocean pH, Proc. Natl. Acad. Sci., 119, e2118009119, https://doi.org/10.1073/pnas.2118009119, 2022.

Kroeker, K. J., Micheli, F., and Gambi, M. C.: Ocean acidification causes ecosystem shifts via altered competitive interactions, Nat. Clim. Change, 3, 156–159, https://doi.org/10.1038/nclimate1680, 2012.

Kwiatkowski, L., Gaylord, B., Hill, T., Hosfelt, J., Kroeker, K. J., Nebuchina, Y., Ninokawa, A., Russell, A. D., Rivest, E. B., Sesboüé, M., and Caldeira, K.: Nighttime dissolution in a temperate coastal ocean ecosystem increases under acidification, Sci. Rep., 6, 22984, https://doi.org/10.1038/srep22984, 2016.

Kwiatkowski, L., Torres, O., Bopp, L., Aumont, O., Chamberlain, M., Christian, J. R., Dunne, J. P., Gehlen, M., Ilyina, T., John, J. G., Lenton, A., Li, H., Lovenduski, N. S., Orr, J. C., Palmieri, J., Santana-Falcón, Y., Schwinger, J., Séférian, R., Stock, C. A., Tagliabue, A., Takano, Y., Tjiputra, J., Toyama, K., Tsujino, H., Watanabe, M., Yamamoto, A., Yool, A., and Ziehn, T.: Twenty-first century ocean warming, acidification, deoxygenation, and upper-ocean nutrient and primary production decline from CMIP6 model projections, Biogeosciences, 17, 3439–3470, https://doi.org/10.5194/bg-17-3439-2020, 2020.

Legrand, E., Riera, P., Pouliquen, L., Bohner, O., Cariou, T., and Martin, S.: Ecological characterization of intertidal rockpools: Seasonal and diurnal monitoring of physico-chemical parameters, Reg. Stud. Mar. Sci., 17, 1–10, https://doi.org/10.1016/j.rsma.2017.11.003, 2018a.

Legrand, E., Riera, P., Bohner, O., Coudret, J., Schlicklin, F., Derrien, M., and Martin, S.: Impact of ocean acidification and warming on the productivity of a rock pool community, Mar. Environ. Res., 136, 78–88, https://doi.org/10.1016/j.marenvres.2018.02.010, 2018b.

Legrand, E., Riera, P., Lutier, M., Coudret, J., Grall, J., and Martin, S.: Grazers increase the sensitivity of coralline algae to ocean acidification and warming, J. Sea Res., 148–149, 1–7, https://doi.org/10.1016/j.seares.2019.03.001, 2019.

Lorenzen, S.: The limpet *Patella vulgata* L. at night in air: effective feeding on *Ascophyllum nodosum* monocultures and stranded seaweeds, J. Molluscan Stud., 73, 267–274, https://doi.org/10.1093/mollus/eym022, 2007.

Mackey, K. R. M., Morris, J. J., Morel, F. M. M., and Kranz, S. A.: Response of photosynthesis to ocean acidification, Oceanography, 28, 74–91, 2015.

Maneveldt, G. W., Wilby, D., Potgieter, M., and Hendricks, M. G. J.: The role of encrusting coralline algae in the diets of selected intertidal herbivores, J. Appl. Phycol., 18, 619–627, https://doi.org/10.1007/s10811-006-9059-1, 2006.

Martin, S., Cohu, S., Vignot, C., Zimmerman, G., and Gattuso, J.-P.: One-year experiment on the physiological response of the Mediterranean crustose coralline alga, *Lithophyllum cabiochae*, to elevated pCO_2 and temperature, Ecol. Evol., 3, 676–693, https://doi.org/10.1002/ece3.475, 2013a.

Martin, S., Charnoz, A., and Gattuso, J.-P.: Photosynthesis, respiration and calcification in the Mediterranean crustose coralline alga *Lithophyllum cabiochae* (Corallinales, Rhodophyta), Eur. J. Phycol., 48, 163–172, https://doi.org/10.1080/09670262.2013.786790, 2013b.

Miller, C. A. and Kelley, A. L.: Alkalinity cycling and carbonate chemistry decoupling in seagrass mystify processes of acidification mitigation, Sci. Rep., 11:13500, https://doi.org/10.1038/s41598-021-92771-2, 2021.

Morris, S. and Taylor, A. C.: Diurnal and seasonal variation in physico-chemical conditions within intertidal rock pools, Estuar. Coast. Shelf Sci., 17, 339–355, https://doi.org/10.1016/0272-7714(83)90026-4, 1983.

Nash, M. C., Diaz-Pulido, G., Harvey, A. S., and Adey, W.: Coralline algal calcification: A morphological and process-based understanding, PLOS ONE, 14, e0221396, https://doi.org/10.1371/journal.pone.0221396, 2019.

Noisette, F., Egilsdottir, H., Davoult, D., and Martin, S.: Physiological responses of three temperate coralline algae from contrasting habitats to near-future ocean acidification, J. Exp. Mar. Biol. Ecol., 448, 179–187, https://doi.org/10.1016/j.jembe.2013.07.006, 2013.

Paiva, F., Brennecke, D., Pansch, C., and Briski, E.: Consistency of aquatic enclosed experiments: The importance of scale and ecological complexity, Divers. Distrib., 27, 524–532, 2021.

Pan, T.-C. F., Applebaum, S. L., and Manahan, D. T.: Experimental ocean acidification alters the allocation of metabolic energy, Proc. Natl. Acad. Sci. U. S. A., 112, 4696–701, https://doi.org/10.1073/pnas.1416967112, 2015.

Pansch, A., Winde, V., Asmus, R., and Asmus, H.: Tidal benthic mesocosms simulating future climate change scenarios in the field of marine ecology, Limnol. Oceanogr. Methods, 14, 257–267, https://doi.org/10.1002/lom3.10086, 2016.

Pinheiro, J., Bates, D., and R-core: Package “nlme”: Linear and Nonlinear Mixed Effects Models, Cran-R, 2018.

R Core Team: R: A language and environment for statistical computing, 2017.

Raven, J. A.: Effects on marine algae of changed seawater chemistry with increasing atmospheric CO_2, Biol. Environ. Proc. R. Ir. Acad., 111B, 1–17, 2011.

Riebesell, U., Czerny, J., von Bröckel, K., Boxhammer, T., Büdenbender, J., Deckelnick, M., Fischer, M., Hoffmann, D., Krug, S. A., Lentz, U., Ludwig, A., Muche, R., and Schulz, K. G.: Technical Note: A mobile sea-going mesocosm system – new opportunities for ocean change research, Biogeosciences, 10, 1835–1847, https://doi.org/10.5194/bg-10-1835-2013, 2013.

Ries, J. B.: Skeletal mineralogy in a high-CO_2 world, J. Exp. Mar. Biol. Ecol., 403, 54–64, https://doi.org/10.1016/j.jembe.2011.04.006, 2011.

Ries, J. B., Ghazaleh, M. N., Connolly, B., Westfield, I., and Castillo, K. D.: Impacts of seawater saturation state (ΩA=0.4–4.6) and temperature (10, 25°C) on the dissolution kinetics of whole-shell biogenic carbonates, Geochim. Cosmochim. Acta, 192, 318–337, https://doi.org/10.1016/j.gca.2016.07.001, 2016.

Schaal, G. and Grall, J.: Microscale aspects in the diet of the limpet Patella vulgata L., J. Mar. Biol. Assoc. U. K., 95, 1155–1162, https://doi.org/10.1017/S0025315415000429, 2015.

Schulz, K. G., Bellerby, R. G. J., Brussaard, C. P. D., Büdenbender, J., Czerny, J., Engel, A., Fischer, M., Koch-Klavsen, S., Krug, S. A., Lischka, S., Ludwig, A., Meyerhöfer, M., Nondal, G., Silyakova, A., Stuhr, A., and Riebesell, U.: Temporal biomass dynamics of an Arctic plankton bloom in response to increasing levels of atmospheric carbon dioxide, Biogeosciences, 10, 161–180, https://doi.org/10.5194/bg-10-161-2013, 2013.

Smith, S. V. and Key, G. S.: Carbon dioxide and metabolism in marine environments, Limnol. Oceanogr., 20, 493–495, https://doi.org/10.4319/lo.1975.20.3.0493, 1975.

Spisla, C., Taucher, J., Bach, L. T., Haunost, M., Boxhammer, T., King, A. L., Jenkins, B. D., Wallace, J. R., Ludwig, A., Meyer, J., Stange, P., Minutolo, F., Lohbeck, K. T., Nauendorf, A., Kalter, V., Lischka, S., Sswat, M., Dörner, I., Ismar-Rebitz, S. M. H., Aberle, N., Yong, J. C., Bouquet, J.-M., Lechtenbörger, A. K., Kohnert, P., Krudewig, M., and Riebesell, U.: Extreme levels of ocean acidification restructure the plankton community and biogeochemistry of a temperate coastal ecosystem: A mesocosm study, Front. Mar. Sci., 7:611157, 2021.

Stumpp, M., Hu, M. Y., Casties, I., Saborowski, R., Bleich, M., Melzner, F., and Dupont, S.: Digestion in sea urchin larvae impaired under ocean acidification, Nat. Clim. Change, 3, 1044–1049, https://doi.org/10.1038/nclimate2028, 2013.

Sulpis, O., Lauvset, S. K., and Hagens, M.: Current estimates of K1* and K2* appear inconsistent with measured CO_2 system parameters in cold oceanic regions, Ocean Sci., 16, 847–862, https://doi.org/10.5194/os-16-847-2020, 2020.

Sulpis, O., Jeansson, E., Dinauer, A., Lauvset, S. K., and Middelburg, J. J.: Calcium carbonate dissolution patterns in the ocean, Nat. Geosci., 14, 423–428, https://doi.org/10.1038/s41561-021-00743-y, 2021.

Torres, O., Kwiatkowski, L., Sutton, A. J., Dorey, N., and Orr, J. C.: Characterizing mean and extreme diurnal variability of ocean CO_2 system variables across marine environments, Geophys. Res. Lett., 48, e2020GL090228, https://doi.org/10.1029/2020GL090228, 2021.

884 Widdicombe, S., Dupont, S., and Thorndyke, M.: Laboratory experiments and benthic mesocosm studies,
885 in: Guide to best practices for ocean acidification research and data reporting. U. Riebesell, V. J. Fabry, L.
886 Hansson and J.-P. Gattuso., Publications Office of the European Union, Luxembourg, 2010.

887 Williamson, C. J., Perkins, R., Voller, M., Yallop, M. L., and Brodie, J.: The regulation of coralline algal
888 physiology, an in situ study of *Corallina officinalis* (Corallinales, Rhodophyta), Biogeosciences, 14, 4485–
889 4498, https://doi.org/10.5194/bg-14-4485-2017, 2017.

890 Yamamoto, S., Kayanne, H., Terai, M., Watanabe, A., Kato, K., Negishi, A., and Nozaki, K.: Threshold of
891 carbonate saturation state determined by CO_2 control experiment, Biogeosciences, 9, 1441–1450,
892 https://doi.org/10.5194/bg-9-1441-2012, 2012.

893

Figures with legends -

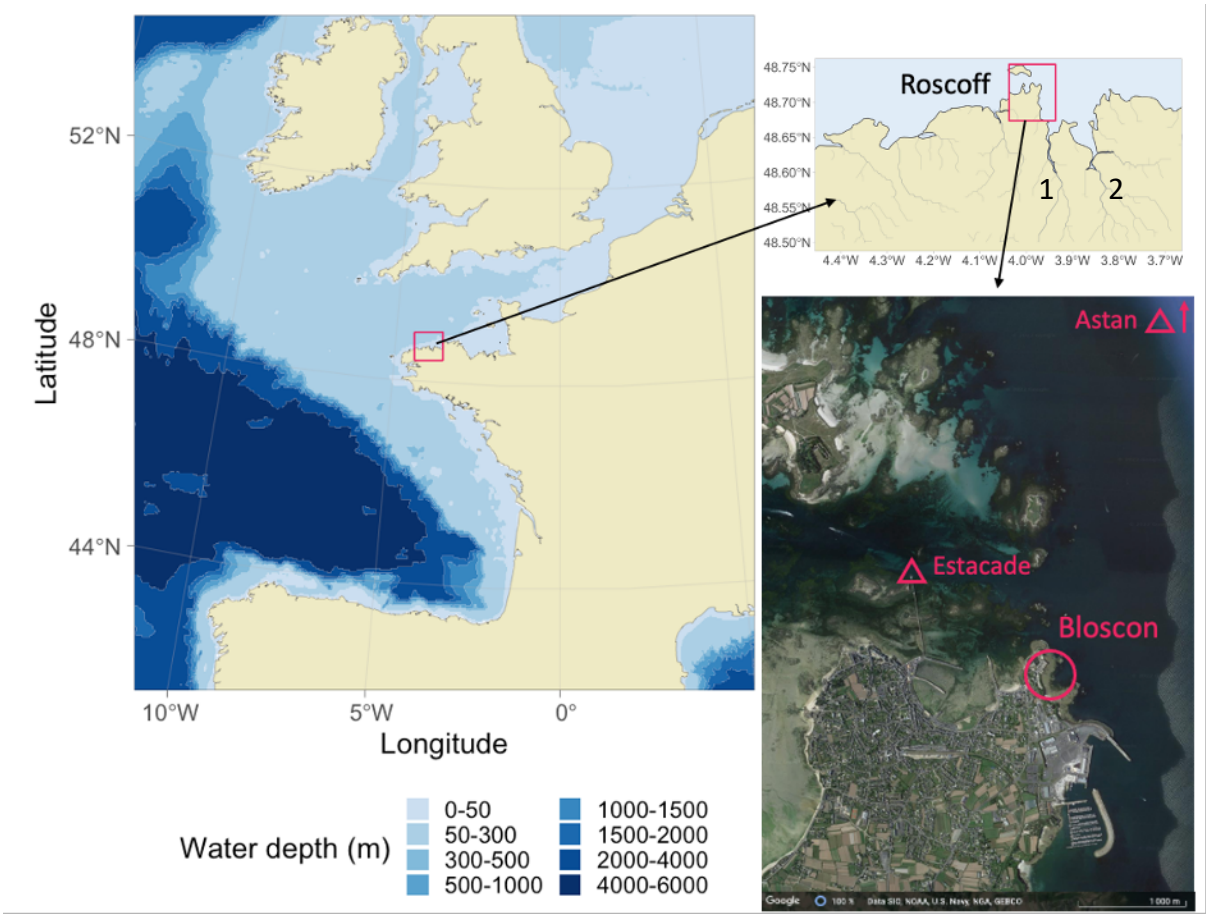

<u>Figure 1 - Field site location</u> on a map of Europe (**left**). The study site (Bloscon) is located in Roscoff, Brittany, France (**right**, top: river mapping data from *HydroSHEDS,* **1**. Penzé river and **2**. Morlaix river; bottom: satellite image from © Google Earth: earth.google.com/web/, acquired in June 2022). The SOMLIT stations Astan and Estacade are indicated with triangles (www.somlit.fr).

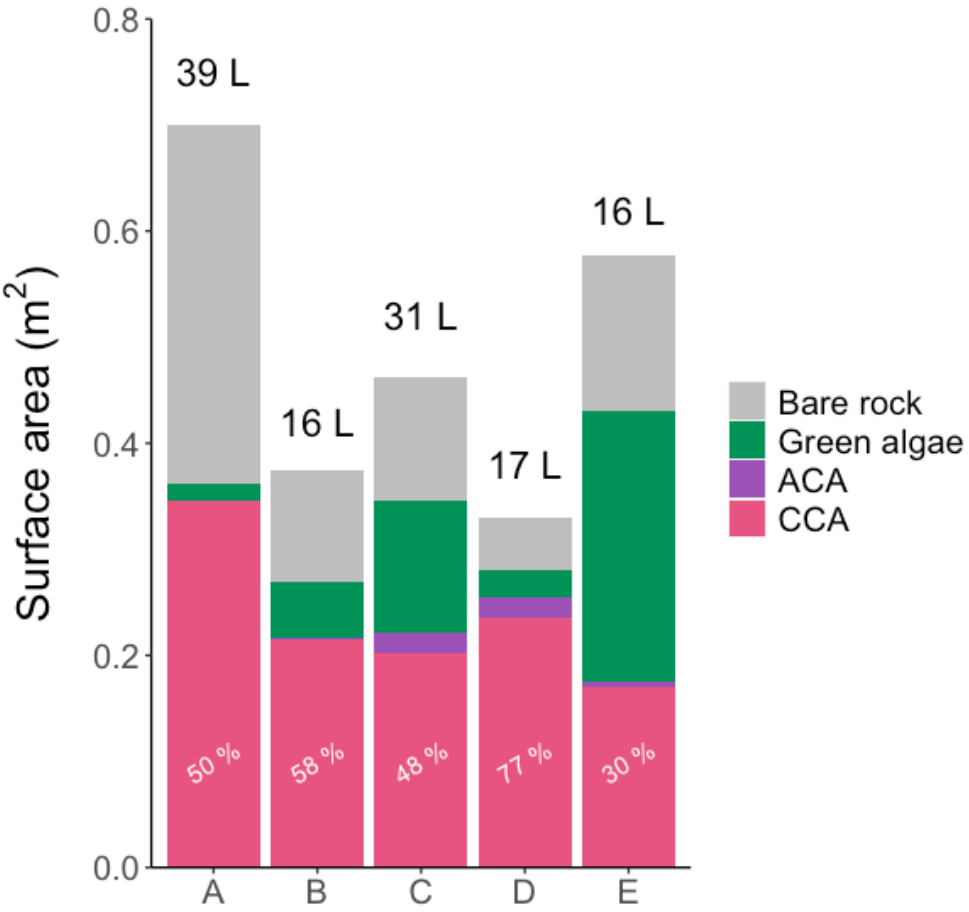

Figure 2 - Pool area, volume and coverage - Surface of the five pools (A-E, September 2020) covered by crustose coralline algae (CCA, pink), articulated coralline algae (ACA, purple) and green algae (green) or free of algae ("bare rock", grey). The length of the bars represents total pool surface area (m^2) and the volume of each pool (L) is indicated above. The relative coverage (%) of calcifying algae (ACA + CCA) in each pool is given. Details for the other seasons are available in **Supp. Mat. Pools Fig. SP1** and **SP2**.

<u>Figure 3</u> - Composite daily pool conditions and biological activity for all pools. A) temperature (°C), **salinity and oxygen concentration** (mg L^{-1}) **and Photosynthetically Active Radiation** (PAR, µmol m^{-2} s^{-1}), **B) pH_T, Total Alkalinity** (TA, µmol kg^{-1}), ***p*CO_2** (µatm), **dissolved inorganic carbon** (DIC, µmol kg^{-1}) **and aragonite saturation state** (Ω_a), and **C) DIC and O_2-derived NCP or CR** (mmol C or O m^{-2} hr^{-1}) **and NCC** (mmol $CaCO_3$ m^{-2} hr^{-1}). Colors represent seasons (**A:** blue for February, orange for April, red for September) and treatment (**B and C**: purple for "present" and green for "future"). Horizontal dotted grey lines represent the mean values of the adjacent ocean. Curves were fitted by season for PAR and for diurnal NCP and NCC using a local polynomial regression (*loess*) with 95% confidence interval. Number of observations: n = 1551 for temperature, salinity and pH_T, n = 1169 for oxygen concentration (data recorded < 22 mg L^{-1}) and n = 632 (hourly data) for the carbonate chemistry parameters, NCC and NCP or CR (**B**). All pools are shown.

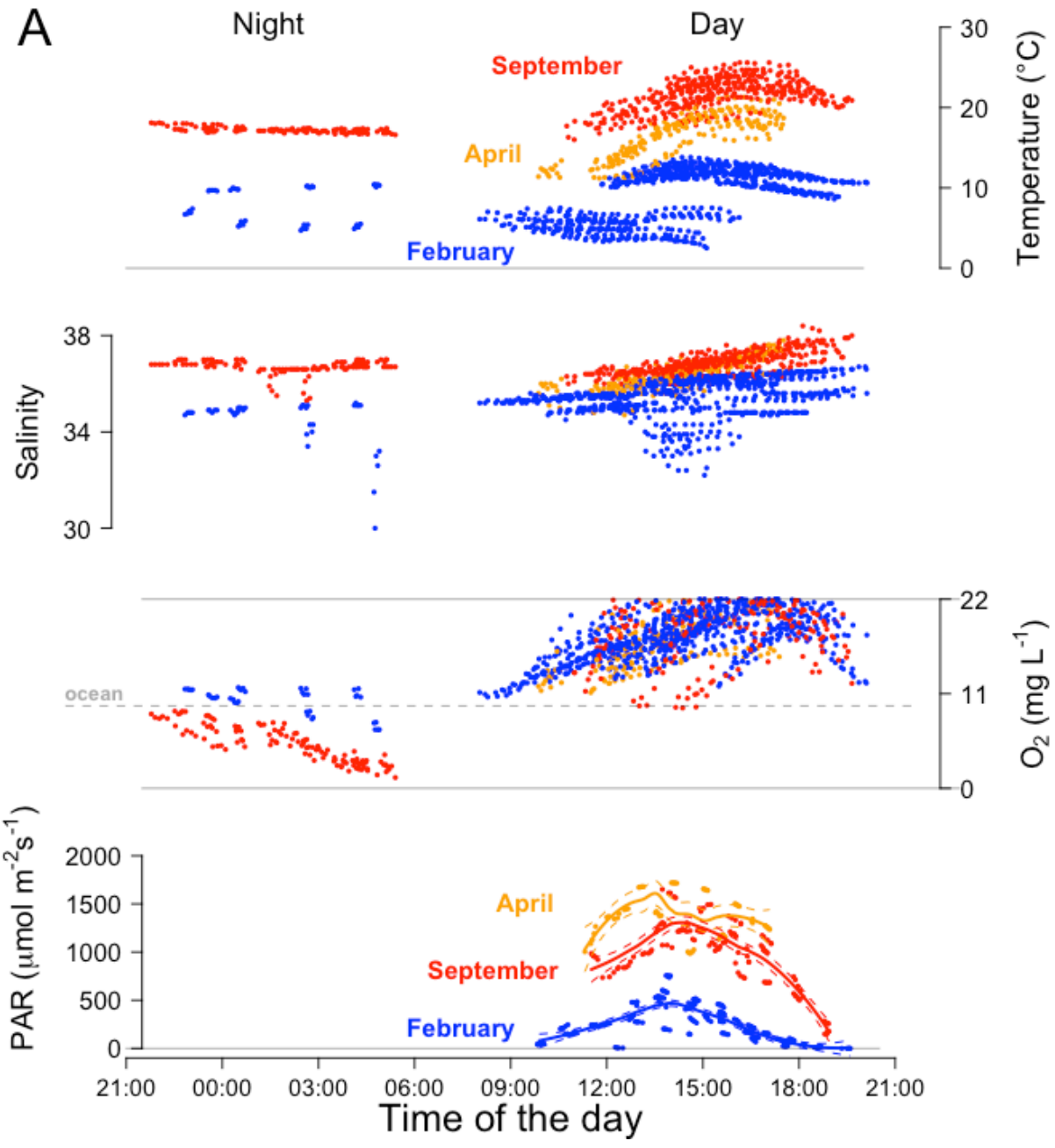

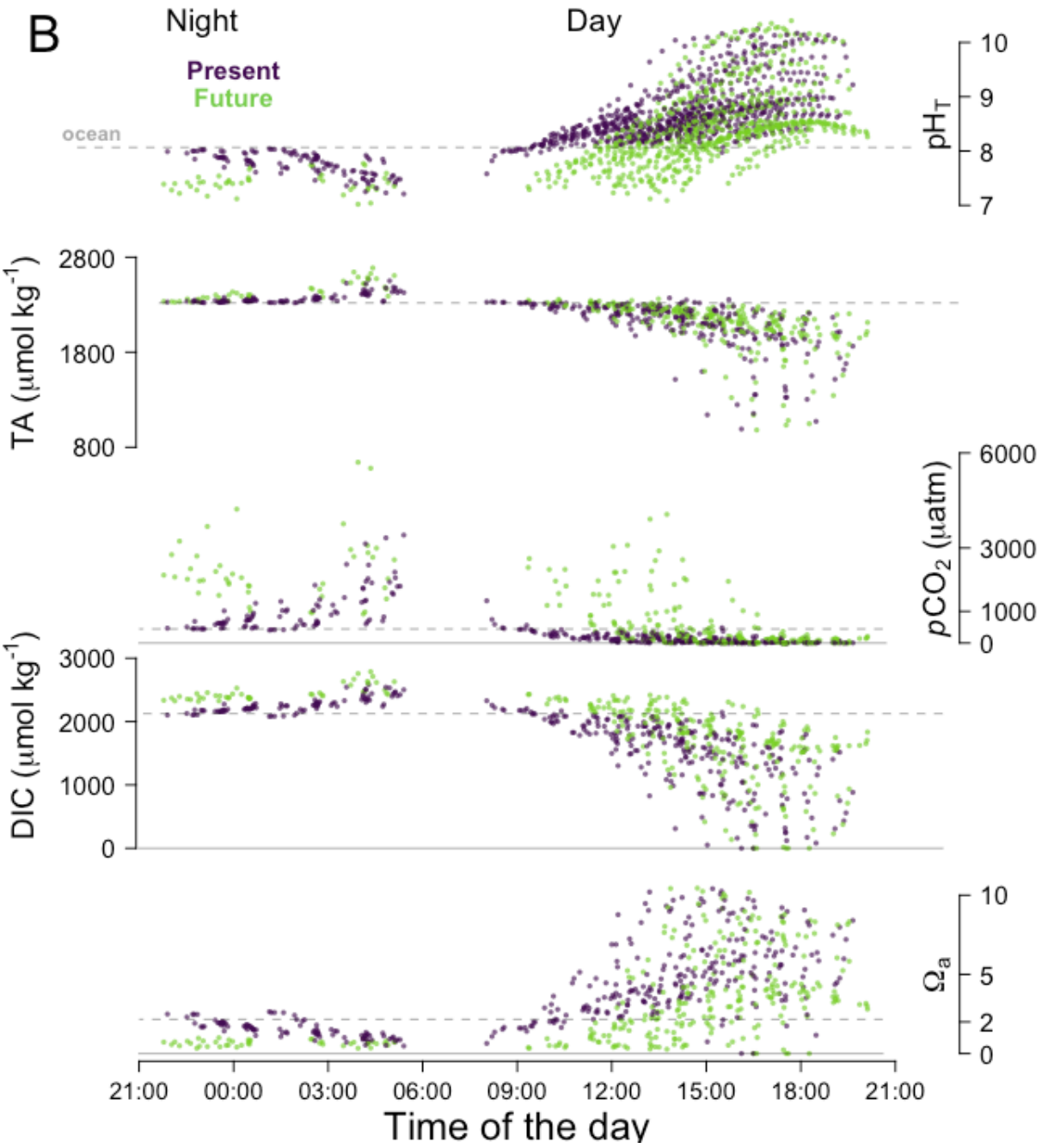
B
Night
Day
Present
Future
ocean
pH_T
10
9
8
7
TA (µmol kg^{-1})
2800
1800
800
pCO_2 (µatm)
6000
3000
1000
0
DIC (µmol kg^{-1})
3000
2000
1000
0
Ω_a
10
5
2
0
21:00
00:00
03:00
06:00
09:00
12:00
15:00
18:00
21:00
Time of the day

25

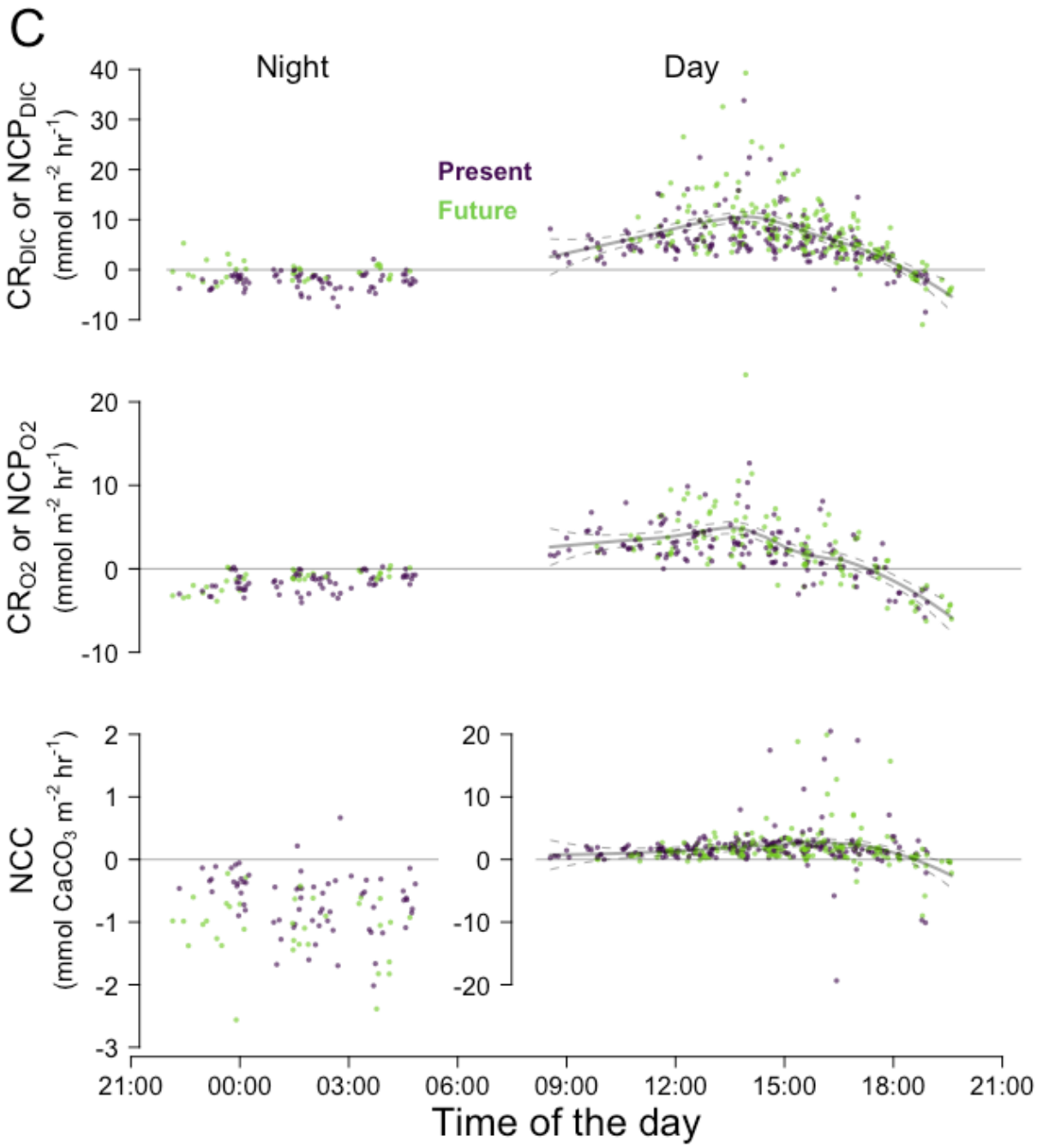
C
Night
Day
Present
Future
CR_{DIC} or NCP_{DIC} (mmol m^{-2} hr^{-1})
CR_{O2} or NCP_{O2} (mmol m^{-2} hr^{-1})
NCC (mmol $CaCO_3$ m^{-2} hr^{-1})
40
30
20
10
0
-10
20
10
0
-10
2
1
0
-1
-2
-3
20
10
0
-10
-20
21:00
00:00
03:00
06:00
09:00
12:00
15:00
18:00
21:00
Time of the day

26

27

Figure 4 – A) O_2-derived (white boxes) and DIC-derived (colored boxes) NCP_{lm} (mmol m^{-2} hr^{-1}), and B) NCC_{lm} (mmol $CaCO_3$ m^{-2} hr^{-1}) during the day and night (shaded areas), by season and by treatment (purple for "present" and green for "future") – Rates are presented as boxplots showing median, 1st and 3rd quartile and 1.5 inter-quartile range (bars), with overlayed individual observations (round symbols). Individual rates were calculated for each pool, each tide and each treatment: n = 50 (FEB-day), n = 10 (FEB-night), n = 10 (APR-Day), n = 25 (SEP-Day), n = 20 (SEP-Night). Seasons: FEB for winter (pooled February 2020 and 2021), APR for spring (April 2021) and SEP for summer (pooled September 2020 and 2021). *Note that for NCC_{lm}, nights (<0) and days (>0) have different y-axis scales for better visualization of night differences. Statistical details of the linear regressions can be found in the corresponding* ***Supplementary Materials****. For O_2-derived NCP_{lm}, in September, three rates were out of the range plotted and their values are indicated next to the small arrow.*

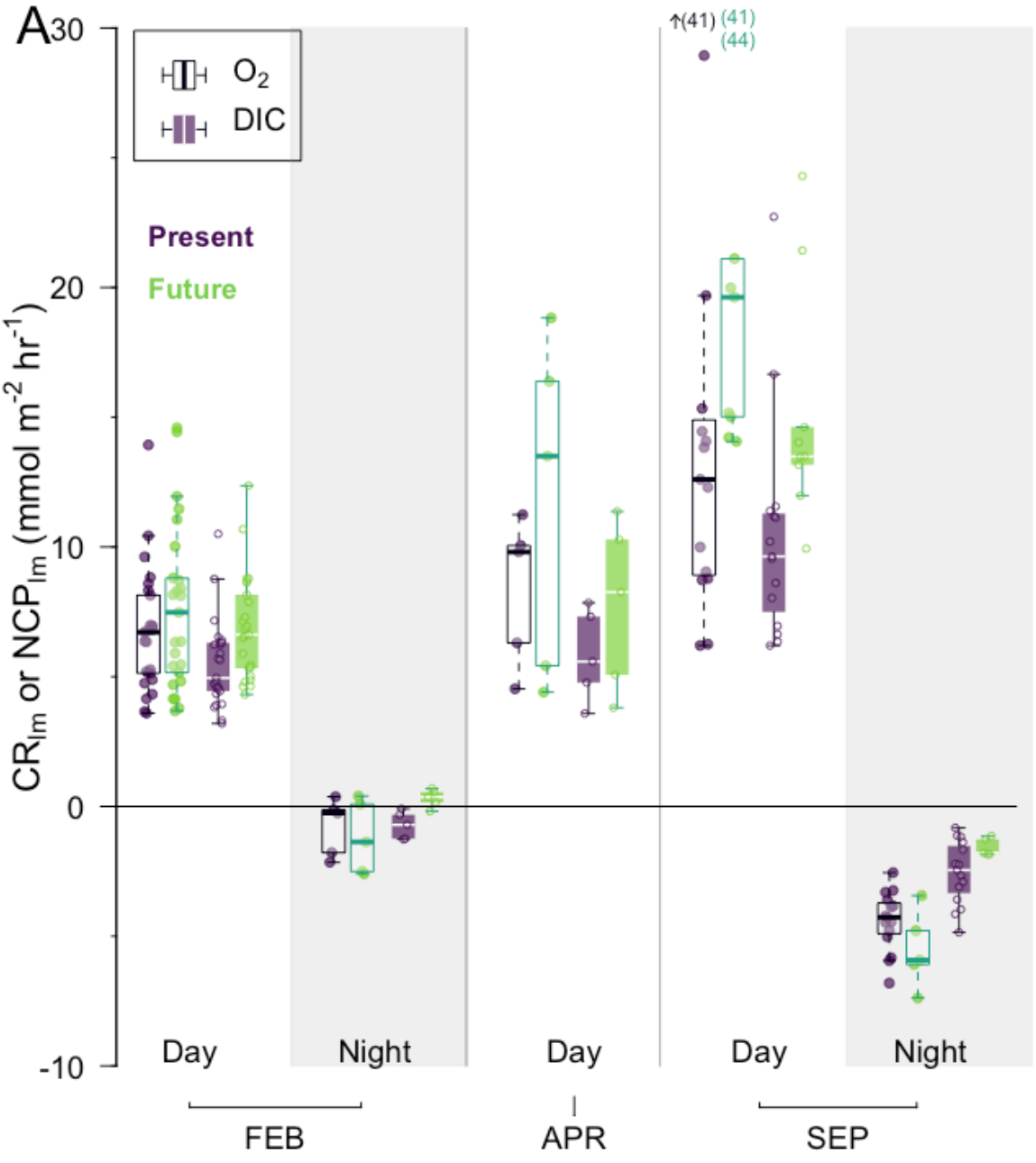

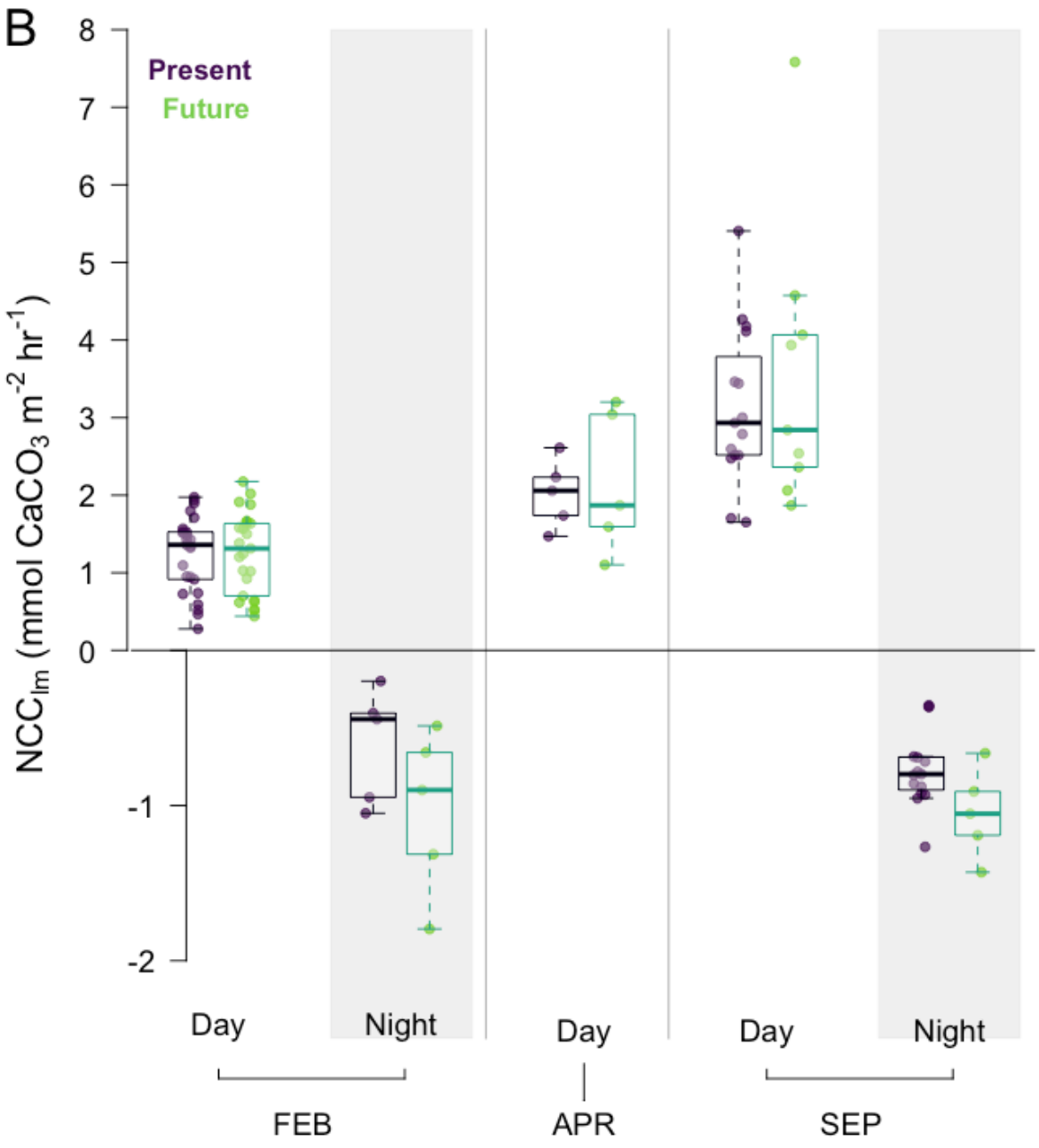
B
Present
Future
8
7
6
5
4
3
2
1
0
-1
-2
NCC$_{lm}$ (mmol CaCO$_3$ m^{-2} hr^{-1})
Day
Night
Day
Day
Night
FEB
APR
SEP

41

42

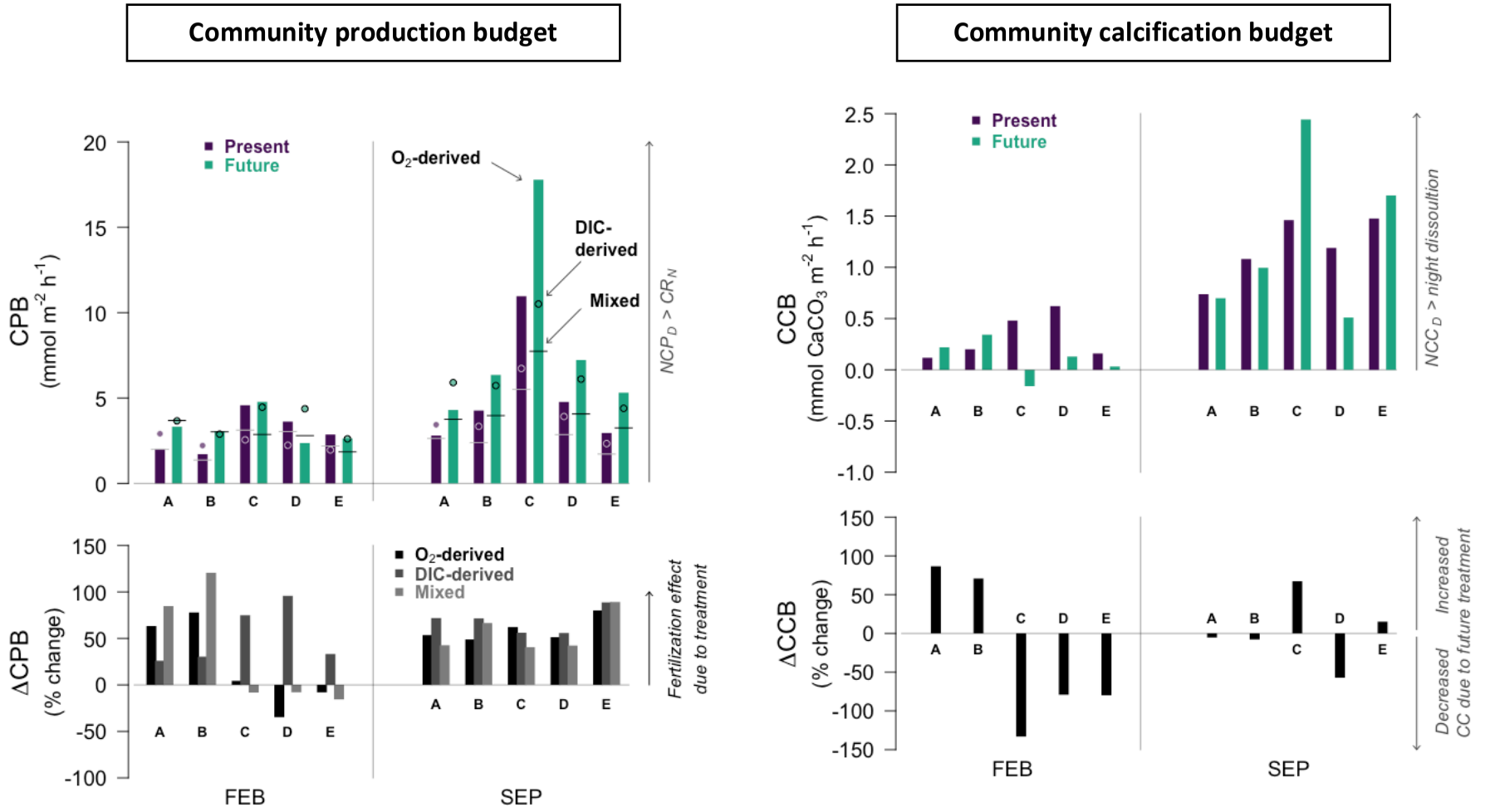

Figure 5 – Community production budget: CPB [1]), and calcification budget: CCB (upper right panel, mmol $CaCO_3$ m^{-2} hr-1) by treatment (purple for "present" and green for "future") for each pool and season (same legend as Fig. 4). CPB >0 if diurnal NCP > nocturnal respiration and CCB > 0 if diurnal NCC > nocturnal dissolution. CPB was estimated three different ways: from O_2-derived NCP (bars), from DIC-derived NCP (round symbols) and from nocturnal O_2-derived CR combined with diurnal DIC-derived NCP ("mixed", vertical segments). **The bottom panels present the change (%) of diel production (ΔCPB: left) and diel calcification (ΔCCB: right) due to CO_2 addition.** Positive ΔCPB indicates a fertilization effect due to the CO_2 addition; negative ΔCCB is expected if the CO_2 addition decreases net calcification/increases net dissolution. All three methods to estimate CPB indicate a fertilization effect in summer.

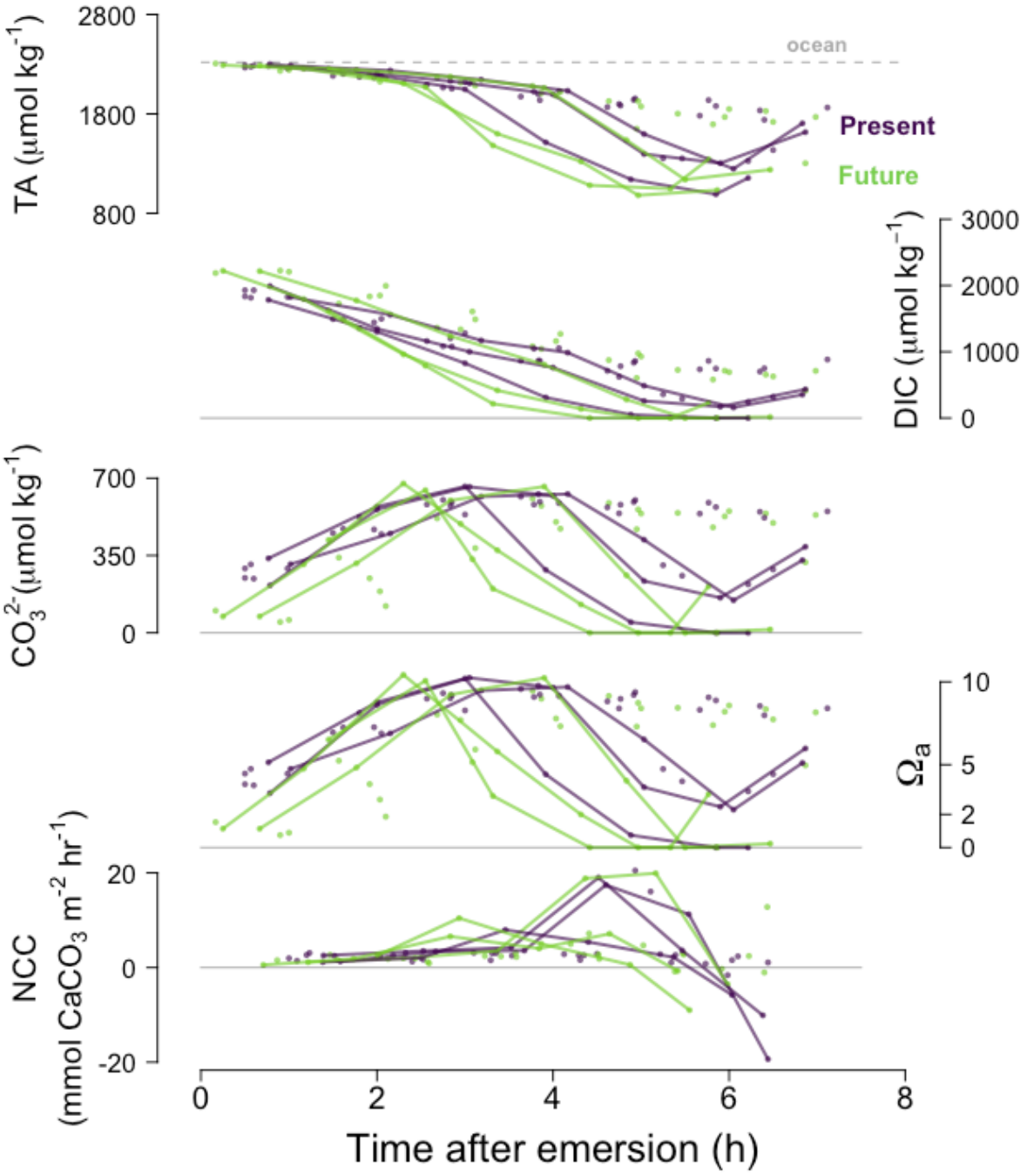

<u>Figure 6 - Time series for September 2020 diurnal data only:</u> A) Total Alkalinity (TA, µmol kg^{-1}), dissolved inorganic carbon, CO_3^{2-} concentration (µmol kg^{-1}), aragonite saturation state (Ω_a) and NCC (mmol m^{-2} hr^{-1}) with time after emersion, by treatment (purple for "present" and green for "future"). The lines in bold represent individual pools C and E that switched from calcification to dissolution when pH_T was still above 9. A similar figure in **Supp. Mat. (Fig. S4)** shows that sunset/irradiance are not correlated with the sudden change towards dissolution.

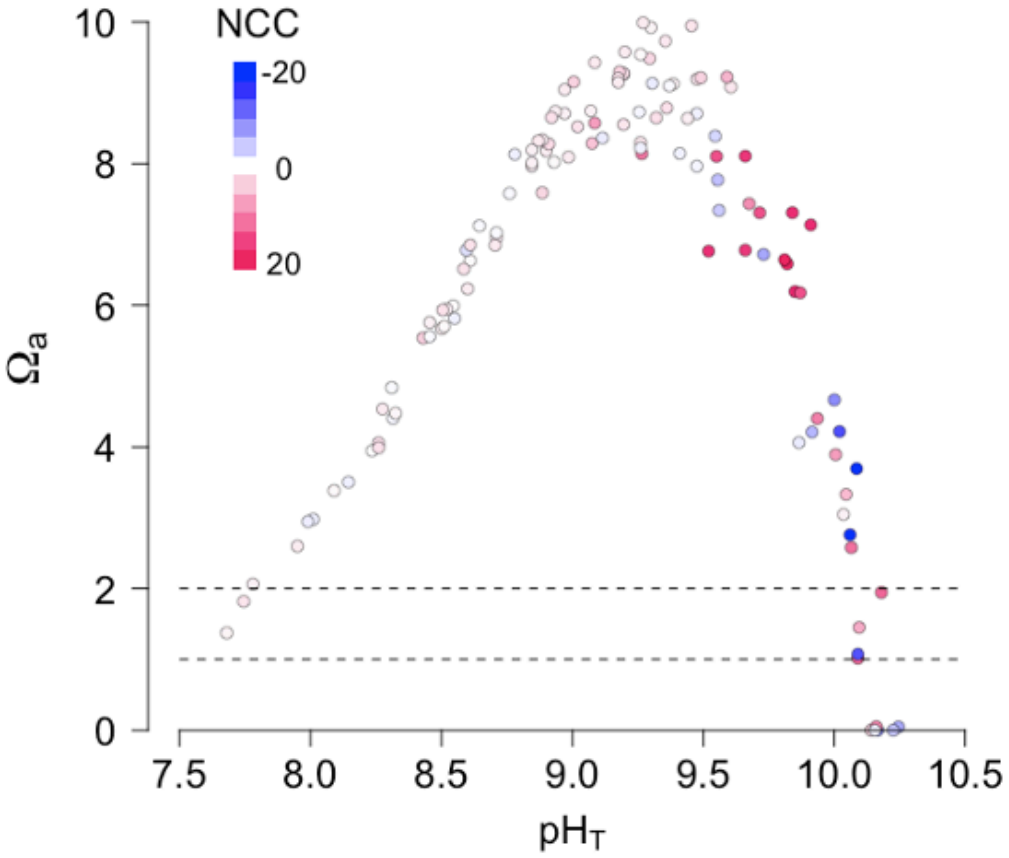

Figure 7 – At very high pH there was both fast net calcification (red) and rapid net dissolution (blue): In some extreme cases, pH_T was not a good indicator or seawater saturation state (Ω_a). Selected dataset of diurnal low-tide emersion periods from September 2020. Colors represent NCC (in mmol $CaCO_3$ m^{-2} hr^{-1}, as presented in **Fig. 3C**). Dashed horizontal lines represent saturation state for aragonite ($\Omega_a = 1$) and for high-Mg calcite ($\Omega_a = 2$).